Cellular/Molecular

Capsaicin Induces Theta-Band Synchronization between Gustatory and Autonomic Insular Cortices

Mitsuru Saito,[1]* Hiroki Toyoda,[1]* Shinpei Kawakami,[1,2]* Hajime Sato,[1]* Yong Chul Bae,[3] and Youngnam Kang[1]

[1]Department of Neuroscience and Oral Physiology, Osaka University Graduate School of Dentistry, Suita, Osaka 565-0871, Japan, [2]Nourishment Function Laboratory, Health Care Division, Morinaga & Company, Ltd., Yokohama, Kanagawa 230-8504, Japan, and [3]Department of Oral Anatomy and Neurobiology, BK21, School of Dentistry, Kyungpook National University, Daegu 700-412, South Korea

In the insular cortex, the primary gustatory area caudally adjoins the primary autonomic area that is involved in visceral sensory-motor integration. However, it has not been addressed whether neural activity in the gustatory insula (Gu-I) is coordinated with that in the autonomic insula (Au-I). We have demonstrated that TRPV1 activation in Gu-I induces theta-band synchronization between Gu-I and Au-I in rat slice preparations. Electron-microscopic immunohistochemistry revealed that TRPV1 immunoreactivity was much higher in Gu-I than in Au-I, and was mostly detected in dendritic spines receiving asymmetrical synapses. Whole-cell voltage-clamp recordings revealed that, in Gu-I, capsaicin-induced currents in layer 3 (L3) pyramidal cells (PCs) displayed no apparent desensitization, while those in layer 5 (L5) PCs displayed Ca^{2+}-dependent desensitization, suggesting that L3 and L5 PCs respond differentially to TRPV1 activation. Voltage-sensitive dye imaging demonstrated that TRPV1 activation in Gu-I can alter an optical response with a monophasic and columnar temporospatial pattern evoked within Gu-I into an oscillatory one extending over Gu-I and Au-I. Power and cross-power spectral analyses of optical responses revealed theta-band synchronization between Gu-I and Au-I. Whole-cell current-clamp recordings demonstrated that such theta-band waves were mediated by sustained rhythmic firings at 4 and 8 Hz in L3 and L5 PCs, respectively. These results strongly suggested that theta-band oscillatory neural coordination between Gu-I and Au-I was induced by two distinct TRPV1-mediated theta-rhythm firings in L3 and L5 PCs in Gu-I. This network coordination induced by TRPV1 activation could be responsible for autonomic responses to tasting and ingesting spicy foods.

Introduction

In the insular cortex, the rostral dysgranular region is involved in taste perception as the primary gustatory area (Yamamoto, 1987; Accolla et al., 2007), while its caudal granular region is potentially involved in visceral sensory-motor control as the primary autonomic area (Ruggiero et al., 1987; Cechetto and Saper, 1990; Yasui et al., 1991). Thus, the gustatory insula (Gu-I) and autonomic insula (Au-I) adjoin rostrocaudally. However, it has not been addressed whether neural activity in Gu-I is coordinated with that in Au-I.

When we taste and ingest hot and spicy foods containing capsaicin, we experience various autonomic responses such as perspiration from the face (Lee, 1954), salivation (Dunér-Engström et al., 1986), and facilitation of cardiovascular activity (Hachiya et al., 2007). Although the exact mechanisms remain unknown, these responses are believed to be induced as a result of viscero-visceral autonomic reflexes (Ganong, 2003). Such reflexes might be caused by impulse activity in oral and gastrointestinal nociceptive afferents resulting from TRPV1 activation by capsaicin in a temperature/pH-dependent manner (Caterina et al., 1997; Tominaga et al., 1998). However, viscero-visceral reflexes might not preclude the possible involvement of higher-order sensory-motor integration between Au-I and Gu-I. Thus, the anatomical arrangement of Gu-I and Au-I together with such autonomic responses to spicy taste led us to investigate whether there exists coordination of neural activity between Gu-I and Au-I.

Although TRPV1 expression in rats was much lower in the cerebral cortex than in nociceptive DRG neurons (Sanchez et al., 2001), the highest TRPV1 expression in the mouse CNS was found in the agranular insular cortex (Roberts et al., 2004), which integrates pain information from peripheral nociceptive neurons (Treede et al., 1999; Jasmin et al., 2004). The mouse granular insular cortex displays similarly high TRPV1 expression (Roberts et al., 2004), but the detailed TRPV1 distribution in its subregions, dysgranular Gu-I and granular Au-I, remains unknown.

In the rat Gu-I, there are a variety of neurons responding to gustatory, tactile, thermal, or nociceptive stimuli applied to the tongue and oral mucosa (Yamamoto et al., 1988; Hanamori et al., 1998) that express TRPV1 (Ishida et al., 2002; Kido et al., 2003). TRPV1 may also be expressed in thermal and/or nociceptive neurons in Gu-I. An fMRI study in human subjects has demonstrated

Received Dec. 31, 2011; revised July 31, 2012; accepted Aug. 7, 2012.

Author contributions: Y.K. designed research; M.S., H.T., S.K., H.S., and Y.C.B. performed research; M.S., H.T., and H.S. analyzed data; Y.K. wrote the paper.

This work was supported by a donation from Morinaga & Company, Ltd., and Grant-in-Aid for Scientific Research (B) 22300127 from the Japanese Ministry of Education, Culture, Sports, Science and Technology (Y.K.), and also supported by Grant for the Basic Science Research Program 2010-0029460 through the National Research Foundation from the Korean Ministry of Education, Science and Technology (Y.C.B.).

The authors declare no competing financial interests.

*M.S., H.T., S.K., and H.S. contributed equally to this work.

Correspondence should be addressed to Dr. Youngnam Kang, Department of Neuroscience and Oral Physiology, Osaka University Graduate School of Dentistry, 1-8, Yamadaoka, Suita, Osaka 565-0871, Japan. E-mail: kang@dent.osaka-u.ac.jp.

DOI:10.1523/JNEUROSCI.5906-11.2012

 0270-6474/12/3213470-18$15.00/0

that the tasting and swallowing of capsaicin cause excitation in Gu-I (Rudenga et al., 2010), suggesting that Gu-I processes the sensory information of hot and spicy taste of capsaicin. It can therefore be hypothesized that TRPV1 in Gu-I is involved in the perception of hot and spicy taste, similar to the putative important role of TRPV1 in the agranular insular cortex in central pain processing.

In the present study, we first investigated whether TRPV1 is differentially distributed in Gu-I and Au-I and subsequently examined whether the activation of TRPV1 in Gu-I induces neural coordination between Gu-I and Au-I. Using voltage-sensitive dye imaging and whole-cell recording, we found that theta-band synchronization between Gu-I and Au-I was induced by two distinct TRPV1-mediated theta-rhythm firings in supragranular and infragranular pyramidal cells in Gu-I.

Materials and Methods

All experiments were performed in accordance with the guidelines of the animal ethics committees of our institutions for the care and use of laboratory animals.

Electron-microscopic immunohistochemistry. Three male Sprague Dawley rats weighing 300–320 g were used for this study. The rats were deeply anesthetized with sodium pentobarbital (80 mg/kg, i.p.) and perfused transcardially with 100 ml of heparinized normal saline followed by 500 ml of freshly prepared mixture of 4% paraformaldehyde and 0.01% glutaraldehyde in 0.1 M phosphate buffer (PB), pH 7.4. Cerebral cortex including insula between 2.0 and −0.8 mm from bregma was removed and postfixed in the same fixative for 2 h at 4°C. Sections were cut transversely on a Vibratome at 60 μm and cryoprotected in 30% sucrose in PB overnight at 4°C.

Sections were frozen on dry ice for 20 min and thawed in 0.01 M PBS, pH 7.2, to enhance penetration, and pretreated with 1% sodium borohydride for 30 min to remove glutaraldehyde. Sections were then blocked with 3% H_2O_2 for 10 min to suppress endogenous peroxidases, and with 10% normal donkey serum (Jackson ImmunoResearch) for 30 min to mask secondary antibody binding sites. For single immunostaining for TRPV1, sections were incubated overnight in goat anti-TRPV1 antibody (1:300; sc-12498; Santa Cruz Biotechnology) at 4°C and, the next day, rinsed in PBS for 15 min and incubated for 2 h in biotinylated donkey anti-goat antibody (1:200; Jackson ImmunoResearch). After washing, the sections were incubated with ExtrAvidin peroxidase (1:5000; Sigma-Aldrich) for 1 h, and the immunoperoxidase was visualized by nickel-intensified 3,3′-diaminobenzidine tetrahydrochloride (DAB). Sections were osmicated in osmium tetroxide (1% in PB) for 1 h, dehydrated in graded alcohols, flat embedded in Durcupan ACM Fluka (Sigma-Aldrich) between strips of ACLAR plastic film (Electron Microscopy Sciences), and cured for 48 h at 60°C. Trapezoidal chips in superficial or deep layer of the insular cortex were cut out of the wafers and glued onto blank resin blocks with cyanoacrylate (see Fig. 2*Aa*,*Ab*). Thin sections were cut with a diamond knife, mounted on Formvar-coated single-slot nickel grids and stained with uranyl acetate and lead citrate. Grids were examined on an electron microscope (H-7500; Hitachi High Technologies). Images were captured by a cooled CCD camera (SC1000; Gatan). The specificity of primary antibody was confirmed by omitting the primary antibody in processing sections and by examining the consistency of immunostaining in adjacent serial thin sections of the same dendrites or terminals. Staining was eliminated by preincubation of the diluted antiserum (1:500) with blocking peptide (sc-12498P; Santa Cruz Biotechnology) at a concentration of 46 μg/ml. We also observed no staining with this antibody on material from *TRPV1*$^{-/-}$ mice (The Jackson Laboratory).

To assess the density of TRPV1-immunopositive neuropils, each of three randomly selected areas (839.1 μm^2) in respective layer 2/3 and layer 5 of the insular cortex in a rat was subdivided into a matrix of 5 × 6 small square areas, from which 30 electron micrographs (27.97 μm^2 each; 30,000×) were captured. Numbers of TRPV1-immunopositive neuropils in electron micrograph were counted and summed over the 30 electron micrographs in each area, and the respective numbers of TRPV1-immunopositive neuropils obtained from the nine areas (three randomly selected areas in each of the three rats) were averaged. The density of TRPV1-immunopositive neuropils was defined as the number of TRPV1-immunopositive neuropils per 1000 μm^2.

Slice preparation. Wistar rats of both sexes at 14–22 d of age were used. Coronal sections of the Gu-I were cut at 300 μm thick for whole-cell voltage-clamp recording. For voltage-sensitive dye (VSD) imaging and whole-cell current-clamp recording, slice preparations, namely tilted-horizontal slices, were cut along the rhinal fissure (RF) in a plane tilted up at 15° to the horizontal plane at 350 μm thick, to include the agranular insula (AI), the dysgranular insula (DI), and the granular insula (GI) by referring to the middle cerebral artery (MCA) (Fig. 1) (Accolla et al., 2007). GI has recently been reclassified as GI/DI (Paxinos and Watson, 1998). DI represents the gustatory area (Gu-I), and GI/DI represents the autonomic area (Au-I). Caudal end of Au-I is located at 2.0 mm caudal to MCA (Cechetto and Saper, 1987). In the experiments using VSD imaging or whole-cell current-clamp recording, all the data were obtained from the tilted-horizontal slices, the bottom surface of which was located 350 μm dorsal to RF. When three serial sections of 100 μm thickness cut at the levels between 350 and 650 μm dorsal to RF were examined using Nissl staining in the 10 rats examined, the boundary between DI and GI/DI that was determined based on the thickness of the granular layer was consistently found to be between 500 and 750 μm caudal to MCA (Fig. 1*Ca*). Similarly, in the living slice preparations of 350 μm thickness, the boundary between Gu-I and Au-I could also be determined based on the thickness of layer 4 that is discernible as a differentially shaded region between layers 2/3 and 5 in either bright-field or resting-light-intensity images. Such a boundary in a living slice was confirmed to be almost the same as that determined in the Nissl-stained image (Fig. 1*D*), which was obtained from the same slice processed for Nissl staining after the slice was fixed overnight in 4% paraformaldehyde and then sectioned on the frozen microtome at 50 μm.

The slices were placed in the recording chamber (volume, 1.0 ml), which was perfused with artificial CSF (ACSF) (in mM: 126 NaCl, 3 KCl, 1 $MgCl_2$, 1.25 NaH_2PO_4, 26 $NaHCO_3$, 2 $CaCl_2$, and 10 D-glucose; pH 7.3) at a flow rate of 1.5 ml/min (=25 μl/s) at room temperature (20–24°C). ACSF was continuously gassed with 95% O_2–5% CO_2.

Whole-cell recordings. The procedures for the whole-cell recordings were previously described (Kang et al., 2007). Whole-cell recordings were obtained from layer 3 (L3) and layer 5 (L5) neurons whose pyramidal shape and proximal apical dendrites were clearly seen at 60× objective under infrared–differential interference contrast microscopy. When recording the current response to capsaicin puff application under voltage-clamp condition, 1 μM tetrodotoxin, 100 μM Ni^{2+}, and 500 μM Cd^{2+} were added in the extracellular solution, in which concentrations of divalent cations were modified in two ways: one containing 0.5 mM Ca^{2+} and 2.5 mM Mg^{2+}, and the other containing 2 mM Ca^{2+} and 1 mM Mg^{2+}. The internal solution had the following composition (in mM): 140 CsCl, 10 HEPES-Na, 2 ATP-Mg, 0.3 GTP-Na_3, 10 EGTA; pH 7.3, adjusted with CsOH. The patch pipettes had a DC resistance of 4–5 MΩ when filled with the internal solution. The sealing resistance was usually >10 GΩ. Under the voltage-clamp condition at the holding potential of −60 mV, a depolarizing ramp pulse from −100 to +50 mV for 1 s was applied during 5 s puff application of 20 μM capsaicin that was repeated every 25 s. Respective amplitudes of inward currents (I_{cap}), evoked by repetitive puff applications of capsaicin, were measured from the baseline current obtained before puff applications. The conductance was measured using linear regression across the linear part of the current–voltage plot (−90 to −20 mV) in response to the ramp pulse. For pooled analysis, respective amplitudes of I_{cap} were normalized to that of the first one, and the conductances (G_{cap}) obtained during capsaicin puff application were normalized to the control conductance. For the current-clamp recordings, the internal solution had the following composition (in mM): 123 K-gluconate, 18 KCl, 14 NaCl, 2 ATP-Mg, 0.3 GTP-Na_3, 10 HEPES, 0.1 EGTA; pH 7.3, adjusted with KOH. Microstimulation (100 μs duration) was delivered via a sharp monopolar tungsten electrode (DC resistance, 0.8–1.8 MΩ) placed at a site 150–450 μm rostral to MCA in layer 4 of Gu-I. Whole-cell currents or voltages were recorded

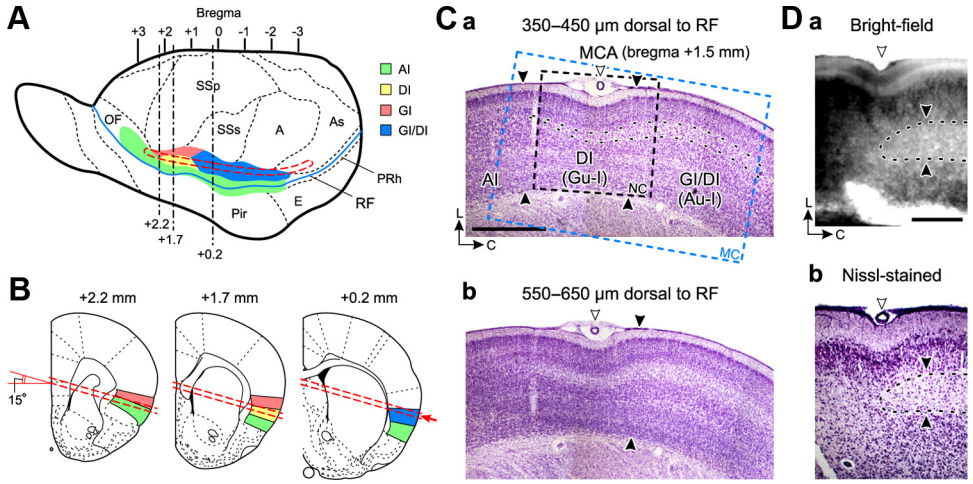

Figure 1. Locations of gustatory and autonomic insular cortices in coronal and horizontal sections. ***A***, A lateral view of rat whole brain modified from a report (Cechetto and Saper, 1987), in which respective regions of the insular cortex are colored differentially. Agranular insula (AI), green; dysgranular insula (DI), yellow; granular insula (GI), orange; hybrid region of GI and DI (GI/DI), blue. Slice preparations were obtained from the region demarcated with a red interrupted line. The blue continuous curve indicates the rhinal fissure (RF). A, Auditory cortex; As, association cortex; E, entorhinal cortex; OF, orbitofrontal cortex; Pir, piriform cortex; PRh, perirhinal cortex; SSp, primary somatosensory cortex; SSs, secondary somatosensory cortex. ***B***, Cross sections of a horizontal slice (red interrupted lines) of the insular cortex at respective levels of coronal brain sections from bregma (Paxinos and Watson, 1998) (see Materials and Methods). ***C***, Microphotographs of Nissl-stained sections of the tilted-horizontal slice (350 μm thick) of the rat insular cortex, at the levels of 350–450 μm (***a***) and 550–650 μm (***b***) dorsal to RF. An open arrowhead indicates MCA. Three distinct regions of the insular cortex were identified based on the thickness of the granular layer, which is demarcated with black interrupted curves. Scale bar, 1 mm. The two pairs of filled facing arrowheads indicate the borders between AI and DI (left pair) and between DI and GI/DI (right pair). The rectangular areas enclosed with black (NC) and blue (MC) interrupted lines indicate the captured areas of voltage-sensitive dye imaging using NeuroCCD-sm (Figs. 5, 6) and MiCAM02-HR (Fig. 7), respectively. L, Lateral; C, caudal. ***D***, The boundary (filled arrowheads) determined in the living slices using bright-field (***a***) was confirmed to be almost the same as that determined in the Nissl-stained image (***b***). The bottom and top parts of the bright-field image were dissimilar from the corresponding parts of the Nissl image, due to an enhancement of contrast of the bright-field image.

with Axopatch 200B (Molecular Devices). Signals were low-pass filtered at 2 kHz (four-pole Bessel filter) and digitized at a sampling rate of 2–10 kHz (Digidata 1322A or 1440A; Molecular Devices). The membrane potential values given in the text were corrected for the liquid junction potential (10 mV) between the K-gluconate-based internal solution (negative) and the standard extracellular solution.

Optical recording using a VSD. The procedures for the optical recording and its data analysis were previously described (Sato et al., 2008). Briefly, the slices were stained with 200 μM RH414 (Invitrogen). The slices were illuminated with light of 535 ± 15 nm wavelength using a stabilized 150 W xenon lamp. The fluorescence emitted from VSD was long-pass filtered above 580 nm and measured with either of the two CCD cameras (NeuroCCD-sm; RedShirtImaging; or MiCAM02-HR; BrainVision), which was attached to a microscope (BX-51WI; Olympus) equipped with a water-immersion objective (10×, 0.3 NA) or an air objective (XLFluor 4×/340, 0.28 NA; Olympus). The imaged area was $1.6 \times 1.6\ mm^2$ (NeuroCCD) or $4.6 \times 3.1\ mm^2$ (MiCAM), and each pixel (element) of the 80 × 80 array (NeuroCCD) or 184 × 124 array (MiCAM) detected the optical signals. The rectangular areas enclosed with black (NC) and blue (MC) interrupted lines indicate the captured areas of voltage-sensitive dye imaging using NeuroCCD (see Figs. 5, 6, 9) and MiCAM02-HR (see Figs. 7, 8), respectively (Fig. 1*Ca*). The fluorescence images were captured at a sampling rate of 125–1000 Hz. Optical responses were analyzed by using NeuroPlex (RedShirtImaging) or BV_Ana (BrainVision), and were displayed as pseudocolor images. Eight series of 512 optical images obtained every 15 s were averaged to improve the signal-to-noise ratio when necessary. No change in fluorescence intensity was observed in the absence of RH414. The threshold current intensity for evoking a columnar spatial pattern of the optical response ranged between 3.2 and 3.7 μA with a mean value of 3.4 μA in coronal slices ($n = 12$) (Sato et al., 2008). This mean value was used as a presumed mean threshold (Th*) in the horizontal slices, because the threshold would not be changed as long as the local circuit is preserved regardless of coronal or horizontal slice preparations. Effects of capsaicin were examined on the spatiotemporal pattern of excitation spread that was induced by stimulation with the current intensity of either 1.2-fold (4 μA) or 1.8-fold (6 μA) presumed mean threshold (1.2 × Th* and 1.8 × Th*, respectively), to be consistent with our previous study (Sato et al., 2008).

Power and cross-power spectral analyses (Sklar et al., 1972) of temporal profiles of optical responses were performed using STATISTICA 10J (StatSoft).

Drug application. Capsaicin (Wako Pure Chemical) and 5′-iodoresiniferatoxin (I-RTX) (Sigma-Aldrich) as an antagonist of TRPV1 were bath-applied at 5–10 and 0.5 μM, respectively. By using a pressure-pulsed microinjector (6–8 psi; PV830; World Precision Instruments), 20 μM capsaicin was puff-applied for 5 s at a flow rate of <0.15 μl/s through a glass pipette. The tip of the glass pipette was placed 50–100 μm above the slice surface and was directed radially to the cortical surface and at an angle of 15–25° to the slice surface to puff capsaicin over the soma-dendritic domain of the recorded cell. Considering the chamber volume (1.0 ml) and the large difference in flow rate between the extracellular solution and the puff-applied capsaicin (25 vs <0.15 μl/s), the concentration of puff-applied capsaicin at a given site on the soma-dendritic domain of the recorded cell would promptly reach a steady level at least several times smaller than 20 μM after the onset of the 5 s puff. The concentrations of bath-applied capsaicin in this study were similar to those used in previous studies on TRPV1 in CNS neurons using slice preparations [≤10 μM (Marinelli et al., 2003); 3 μM (Grueter et al., 2010); ≤10 μM (Cavanaugh et al., 2011)]. Such concentrations are reasonable in view of the dose–response relationship in cultured DRG neurons (EC_{50} = 1.1 μM) (Kim et al., 2006). Phorbol 12-myristate 13-acetate (PMA) (Sigma-Aldrich) was bath-applied at 10 μM, as protein kinase C (PKC) activation by PMA either enhances the capsaicin-induced membrane currents (Vellani et al., 2001; Numazaki et al., 2002) or reverses the desensitization of TRPV1 responses (Mandadi et al., 2006).

Statistical analysis. Numerical data were expressed as the mean ± SD or the geometric mean × [geometric SD] $^{\pm 1}$. The statistical significances in nonpairwise and pairwise experiments were assessed using unpaired (†) and paired (‡) Student's *t* test, respectively, or factorial ($^{\$}$) and repeated-measure ($^{\$}$) ANOVA, respectively, followed by Fisher's protected least significant difference *post hoc* test ($^{\Pi}$) (STATISTICA 10J; StatSoft; Mathematica 8; Wolfram Research). The two-sample Kolmogorov–Smirnov (K-S) test was used to compare two cumulative probability distributions. A value of $p < 0.05$ was considered statistically significant.

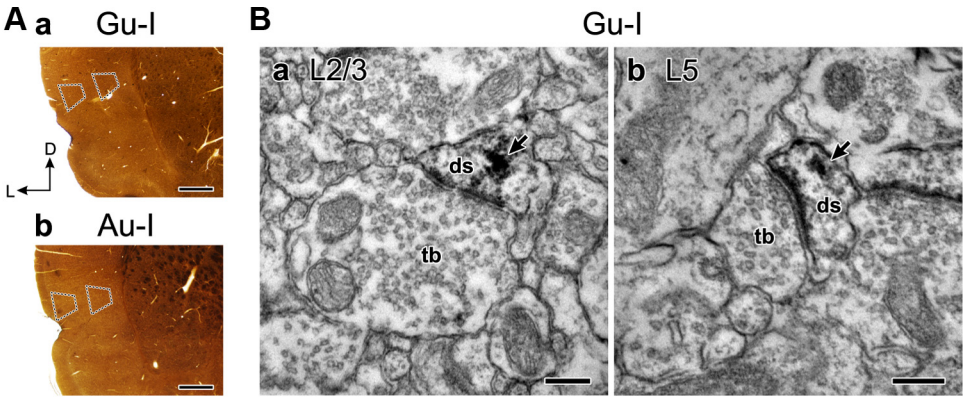

C

Density (per 1,000 μm²)		Postsynaptic: Dendritic spine	Postsynaptic: Dendritic shaft	Presynaptic: Axon terminal
Gu-I	L2/3‡	34.0 ± 1.3†	4.8 ± 1.7	2.1 ± 1.2
	L5‡	17.5 ± 2.0†	2.9 ± 1.6	1.3 ± 0.2
Au-I	L2/3‡	6.7 ± 1.8†	1.9 ± 1.6	1.6 ± 1.1
	L5‡	9.0 ± 1.0†	2.0 ± 1.5	1.9 ± 1.5

Figure 2. Expression of TRPV1 in the rat insular cortex. ***A***, Bright-field images of coronal sections of Gu-I (***a***) and Au-I (***b***) at +1.5 and −0.3 mm from bregma, respectively, in which immunoperoxidase-DAB immunostaining for TRPV1 was performed. The respective trapezoidal areas (dotted lines) localized in the superficial (L2/3) and deep (L5) layers of Gu-I and Au-I show the regions in which the density of TRPV1-immunopositive neuropils was analyzed using electron microscopy. Scale bar, 0.5 mm. L, Lateral; D, dorsal. ***B***, Electron micrographs showing TRPV1-positive postsynaptic dendritic spines (ds) in L2/3 (***a***) and L5 (***b***) of the rat Gu-I. Terminal boutons (tb) making asymmetrical synapses on TRPV1-positive dendritic spines (ds) in L2/3 and L5 of Gu-I. The arrows indicate electron-dense immunoreaction products. Scale bars, 200 nm. ***C***, Density (mean ± SD, per 1000 μm^2) of TRPV1-immunopositive postsynaptic dendrites (spine and shaft) and presynaptic axon terminals in L2/3 and L5 of the rat insular cortex ($n = 9$). $^{\dagger}p < 0.02$; $^{\ddagger}p < 0.001$ (postsynaptic vs presynaptic).

Results

Subcellular distribution of TRPV1 in Gu-I and Au-I

Using an electron-microscopic immunohistochemical method, we first examined whether and how TRPV1 is distributed in Gu-I and Au-I (+1.5 and −0.3 mm from bregma, respectively). In the respective trapezoidal areas in the supragranular and infragranular layers of Gu-I and Au-I (Fig. 2*Aa*,*Ab*), the distribution of TRPV1 was examined. In layers 2/3 (L2/3) and 5 (L5) of Gu-I, TRPV1 immunoreactivity was mostly detected in postsynaptic dendritic spines receiving asymmetrical synapses (Fig. 2*Ba*,*Bb*). As summarized in a table (Fig. 2*C*), the density of TRPV1-immunopositive dendritic spines (per 1000 μm^2; see Materials and Methods) was two times higher in L2/3 (34.0 ± 1.3; $^{\dagger}p < 0.001$) than in L5 (17.5 ± 2.0) in Gu-I. Compared with Gu-I, Au-I expressed much lower TRPV1. The density of TRPV1-immunopositive dendritic spines in L2/3 was five times lower in Au-I (6.7 ± 1.8; $^{\dagger}p < 0.001$) than in Gu-I, while that in L5 was two times lower in Au-I (9.0 ± 1.0; $^{\dagger}p < 0.001$) than in Gu-I (Fig. 2*C*). Thus, TRPV1 was more densely expressed in the dendritic spines of pyramidal cells in Gu-I than in those of pyramidal cells in Au-I.

Capsaicin-induced currents in L3 and L5 PCs in Gu-I

Next, we examined how L3 and L5 pyramidal cells (PCs) in Gu-I respond to puff application of capsaicin under the condition of either 0.5 or 2 mM $[Ca^{2+}]_o$. When 20 μM capsaicin was puff-applied repeatedly to an L3 PC (Fig. 3*Aa*), both capsaicin-induced inward currents (I_{cap}) and current responses to the ramp pulses from −100 to +50 mV for 1 s obtained at 2 mM $[Ca^{2+}]_o$ displayed no apparent desensitization (Fig. 3*Aa*,*Ab*, *1 and *4). The current responses to the ramp pulses obtained before and during puff applications of capsaicin crossed each other at ~0 mV (Fig. 3*Ab*, arrowhead), consistent with the nature of TRPV1 as a nonselective cation channel observed in HEK293 cells (Caterina et al., 1997). With repeated capsaicin puff applications, both the mean values of the peak I_{cap} and of the conductance (G_{cap}) increased in L3 PCs examined at 0.5 mM $[Ca^{2+}]_o$ ($n = 5$) as well as in those examined at 2 mM $[Ca^{2+}]_o$ ($n = 5$) (hollow and solid columns, respectively), while the facilitatory summations of I_{cap} and subsequent increases in G_{cap} were significantly larger ($^{\$}p < 0.05$ and $^{\$}p < 0.01$, respectively) at 2 mM $[Ca^{2+}]_o$ than at 0.5 mM $[Ca^{2+}]_o$ (Fig. 3*Ac*,*Ad*). This result was contrary to the Ca^{2+}-dependent tachyphylaxis or desensitization of TRPV1 in rat DRG neurons (Koplas et al., 1997).

In contrast, in L5 PCs, the first puff application of capsaicin induced a large I_{cap} that desensitized rapidly at 0.5 mM $[Ca^{2+}]_o$ (Fig. 3*Ba*,*Bb*, *1). Subsequent capsaicin puff applications induced no prominent current responses, revealing tachyphylaxis in I_{cap} and in G_{cap} (Fig. 3*Ba*,*Bb*, *3 and *5). Although the difference in the tachyphylaxis of the normalized I_{cap} between L5 PCs examined at 0.5 mM $[Ca^{2+}]_o$ ($n = 5$) and those examined at 2 mM $[Ca^{2+}]_o$ ($n = 5$) was not significant ($^{\$}p > 0.1$), the normalized second I_{cap} was significantly smaller ($^{\dagger}p < 0.05$) at 2 mM $[Ca^{2+}]_o$ (solid column) than at 0.5 mM $[Ca^{2+}]_o$ (hollow column) (Fig. 3*Bc*). The difference in the tachyphylaxis of the normalized G_{cap} was significantly larger ($^{\$}p < 0.02$) at 2 mM $[Ca^{2+}]_o$ than at 0.5 mM $[Ca^{2+}]_o$ (Fig. 3*Bd*). These results suggest an enhancement of tachyphylaxis in I_{cap} and in G_{cap} by a $[Ca^{2+}]_o$ increase. Furthermore, the mean half-duration (0.6 ± 0.6 s; $n = 5$) of the first I_{cap} obtained at 2 mM $[Ca^{2+}]_o$ was significantly shorter ($^{\dagger}p < 0.02$) than that (2.3 ± 1.1 s; $n = 5$) at 0.5 mM $[Ca^{2+}]_o$. These observations are consistent with the Ca^{2+}-dependent desensitization of TRPV1 in rat DRG neurons (Koplas et al., 1997). Thus, the kinetic properties of I_{cap} differ considerably between L3 and L5 PCs.

Effects of PKC activation on I_{cap} in L3 and L5 PCs in Gu-I

PKC activation either enhances the capsaicin-induced membrane currents in rat DRG neurons and heterologous expression systems (Vellani et al., 2001; Numazaki et al., 2002) or reverses

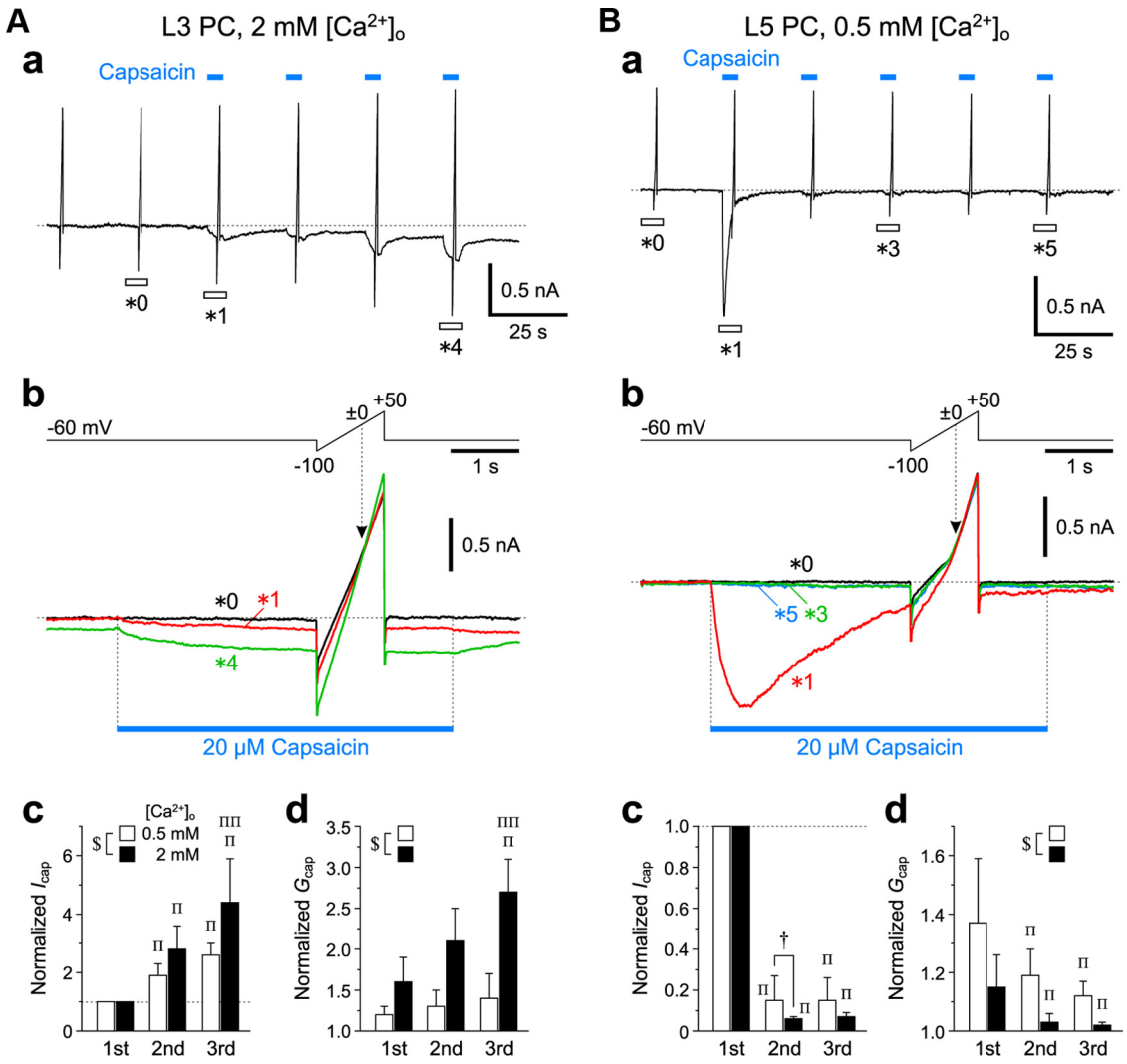

Figure 3. Capsaicin-induced currents in L3 and L5 PCs in Gu-I. ***Aa***, ***Ba***, Sample traces of continuous recordings of inward currents (I_{cap}) induced by 5 s puff application of 20 μM capsaicin and the current responses to the ramp pulses (***Ab***, ***Bb***, top) applied before and during respective puff applications of capsaicin (blue bars), obtained in an L3 PC at 2 mM $[Ca^{2+}]_o$ (***A***) and an L5 PC at 0.5 mM $[Ca^{2+}]_o$ (***B***). Holding potential, −60 mV. ***Ab***, ***Bb***, Top, Positive ramp pulse from −100 to +50 mV for 1 s applied at the holding potential of −60 mV. Bottom, Superimposed enlarged traces of current responses seen during the respective time periods indicated with open horizontal bars in ***Aa*** (*0, *1 and *4) and ***Ba*** (*0, *1, *3 and *5). The blue bars indicate the duration and timing of puff applications of capsaicin. The current responses to the ramp pulse crossed each other at ~0 mV (arrowheads). ***Ac***, ***Bc***, Mean (+SD) amplitudes of I_{cap} obtained in response to the first through the third puff application of capsaicin, normalized to that obtained during the first puff application in L3 PCs at 0.5 mM $[Ca^{2+}]_o$ (hollow columns: second, 1.9 ± 0.4; third, 2.6 ± 0.4; $n = 5$) and in a different set of L3 PCs at 2 mM $[Ca^{2+}]_o$ (solid columns: second, 2.8 ± 0.8; third, 4.4 ± 1.5; $n = 5$) (***Ac***) and those in L5 PCs at 0.5 mM $[Ca^{2+}]_o$ (hollow columns: 0.15 ± 0.12; 0.15 ± 0.11; $n = 5$) and in a different set of L5 PCs at 2 mM $[Ca^{2+}]_o$ (solid columns: 0.06 ± 0.01; 0.07 ± 0.02; $n = 5$) (***Bc***). $^{\dagger}p < 0.05$; $^{\$}p < 0.03$; $^{\Pi}p < 0.05$ (vs First); $^{\Pi\Pi\Pi}p < 0.05$ (vs Second). These symbols are the same as those applied in ***Ad*** and ***Bd***. ***Ad***, ***Bd***, Mean (+SD) values of conductances (G_{cap}) obtained in response to the first through the third puff application of capsaicin, normalized to that obtained in the control conditions in L3 PCs at 0.5 mM $[Ca^{2+}]_o$ (hollow columns: first, 1.2 ± 0.1; second, 1.3 ± 0.2; third, 1.4 ± 0.3; $n = 5$) and in the different set of L3 PCs at 2 mM $[Ca^{2+}]_o$ (solid columns: first, 1.6 ± 0.3; second, 2.1 ± 0.3; third, 2.7 ± 0.3; $n = 5$) (***Ad***) and those in L5 PCs at 0.5 mM $[Ca^{2+}]_o$ (hollow columns: 1.37 ± 0.22; 1.19 ± 0.09; 1.12 ± 0.05; $n = 5$) and in the different set of L5 PCs at 2 mM $[Ca^{2+}]_o$ (solid columns: 1.15 ± 0.11; 1.03 ± 0.03; 1.01 ± 0.01; $n = 5$) (***Bd***).

the desensitization of TRPV1 responses in rat DRG neurons and heterologous expression systems (Mandadi et al., 2004, 2006). Accordingly, we next investigated whether PKC activation is differentially involved in the modulation of the I_{cap} between L3 and L5 PCs. As shown in Figure 3, *Ac*, *Ad*, and *Bc*, *Bd*, both the facilitatory summation of capsaicin-induced currents in L3 PCs and the tachyphylaxis or desensitization of those in L5 PCs were larger at 2 mM $[Ca^{2+}]_o$ than at 0.5 mM $[Ca^{2+}]_o$; therefore, we investigated the effects of PMA on capsaicin-induced currents in L3 and L5 PCs at 2 mM $[Ca^{2+}]_o$.

In an L3 PC, the first puff application of capsaicin in the presence of 10 μM PMA induced a large I_{cap}, concomitantly enhancing the current response to the ramp pulse (Fig. 4*Aa*). The I_{cap} displayed little decay even after the offset of the first puff application (Fig. 4*Aa*). The subsequent puff applications of capsaicin in the presence of PMA induced little inward current ($^{\$}p > 0.3$) and hardly increased the conductances ($^{\$}p > 0.7$) (Fig. 4*Aa–Ad*). These results suggest that, in L3 PCs, both the I_{cap} and G_{cap} attained maximum plateau levels in response to the first puff application of capsaicin in the presence of PMA, most likely due to the strong enhancement of I_{cap} by PKC activation. Similarly, in L5 PCs, the respective puff applications of capsaicin in the presence of PMA induced the respective I_{cap} with little desensitization, which were summated to attain a maximal plateau level (Fig. 4*B*). Subsequently, in L5 PCs, PMA appeared to alleviate the desensitization of I_{cap}, which resulted in the conversion of tachyphylaxis into facilitatory (I_{cap}, $^{\$}p < 0.002$; G_{cap}, $^{\$}p < 0.04$) summation (compare Figs. 4*Bc*,*Bd*, 3*Bc*,*Bd*). Thus, PKC activation

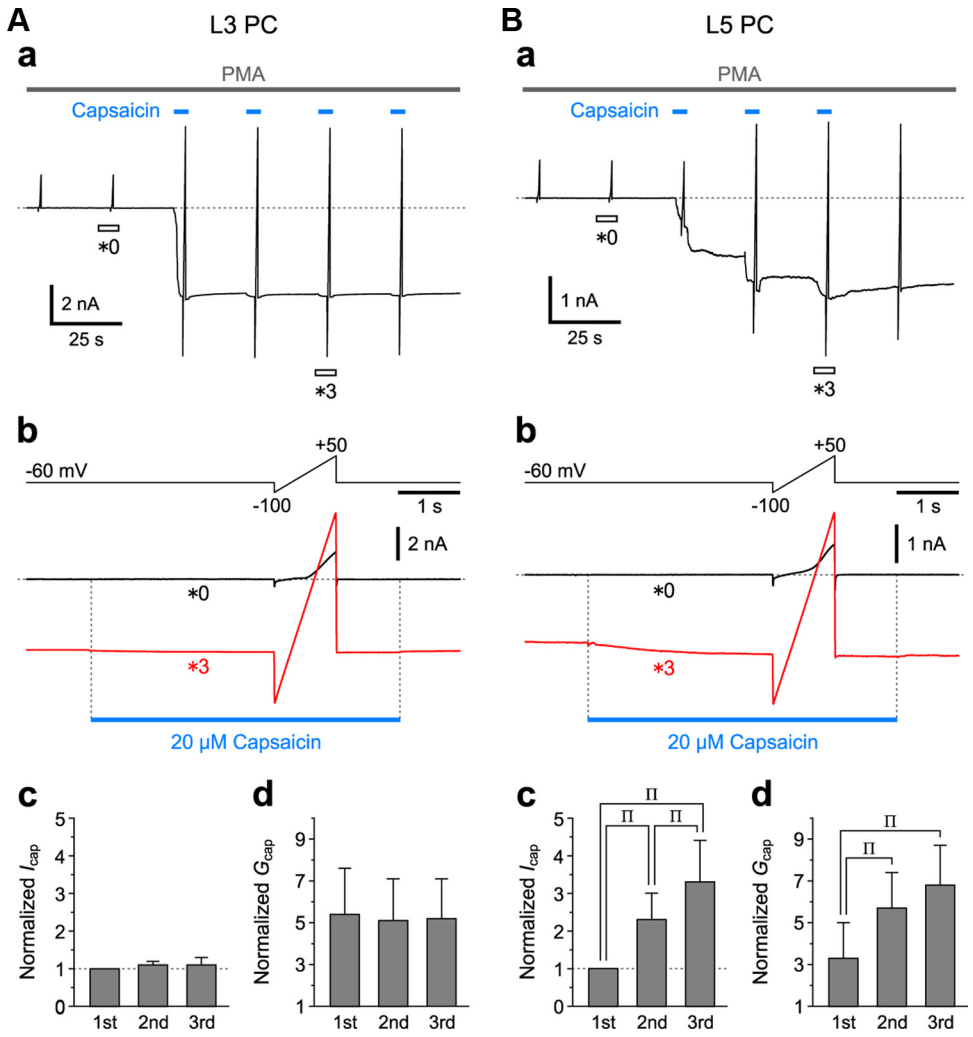

Figure 4. Differential enhancement of capsaicin-induced currents by PKC activation in L3 and L5 PCs in Gu-I. ***Aa***, ***Ba***, Sample traces of continuous recordings of I_{cap} induced by 5 s puff application of 20 μM capsaicin and the current responses to the ramp pulses (***Ab***, ***Bb***, top) applied before and during respective 5 s puff applications of 20 μM capsaicin (blue bars), in the presence of 10 μM PMA in L3 (***A***) and L5 (***B***) PCs at 2 mM $[Ca^{2+}]_o$. Holding potential, −60 mV. ***Ab***, ***Bb***, Top, Positive ramp pulse from −100 to +50 mV for 1 s applied at a holding potential of −60 mV. Bottom, Superimposed enlarged traces of current responses seen during the respective time periods indicated with open horizontal bars in ***Aa*** (*0 and *3) and ***Ba*** (*0 and *3). The blue bars indicate the duration and timing of puff applications of capsaicin. ***Ac***, ***Bc***, Mean (+SD) amplitudes of I_{cap} obtained in response to the first through the third puff application of capsaicin, normalized to that obtained during the first puff application in L3 (second, 1.1 ± 0.1; third, 1.1 ± 0.2; $n = 5$) (***Ac***) and L5 PCs (second, 2.3 ± 0.7; third, 3.3 ± 1.1; $n = 5$) (***Bc***). $^{\Pi}p < 0.05$. ***Ad***, ***Bd***, Mean (+SD) values of G_{cap} obtained in response to the first through the third puff application of capsaicin, normalized to that obtained in the control conditions in L3 (first, 5.4 ± 2.2; second, 5.1 ± 2.0; third, 5.2 ± 1.9; $n = 5$) (***Ad***) and L5 PCs (first, 3.3 ± 1.7; second, 5.7 ± 1.7; third, 6.8 ± 1.9; $n = 5$) (***Bd***). $^{\Pi}p < 0.05$.

changed the TRPV1 response in L5 PCs (Fig. 4*Bc*,*Bd*) to be similar to that in L3 PCs in the absence of PMA (Fig. 3*Ac*,*Ad*).

Effects of capsaicin on columnwise excitation in Gu-I

Using optical imaging, we next examined whether the activation of TRPV1 in L3 and L5 PCs of Gu-I could induce the coordination of neural activity between Gu-I and Au-I in the tilted-horizontal slice preparation (see Materials and Methods). Following stimulation with 4 μA (= 1.2 × Th*) (see Materials and Methods) applied to a site 200 μm rostral to MCA in L4 of Gu-I (Fig. 5*Ca*), an initial optical response was evoked in L4 with a latency of 1 ms (Fig. 5*Aa*, arrowhead), which subsequently spread bidirectionally into L2/3 and L5, displaying a columnar spatial pattern both in the absence and presence of capsaicin (Fig. 5*Aa*,*Ba*, 5–16 ms) in 8 of the 13 slices examined (62%). This columnar excitation slowly faded out in the absence of capsaicin (Fig. 5*Aa*), whereas in the presence of capsaicin, it was followed by a second and third excitation spread extending toward the caudal end of the imaged area of the insular cortex (Fig. 5*Ba*, 103–399 ms), in five of the eight slices.

By referring to the apparent boundary of the optical responses at 5–16 ms after L4 stimulation (Fig. 5*Aa*), we expediently divided the imaged area into four columns (columns 1–4; Fig. 5*Cb*, vertical dotted lines; see Discussion). Columns 1–3 were located in the DI region (Gu-I), and most of column 4 was located in the GI/DI region (Au-I) (Fig. 5*Ca*,*Cb*; also see Fig. 1*C*). The optical responses evoked at the regions of interest (ROIs) (Fig. 5*Cb*) in L3 and L5 in columns 1–3 by L4 stimulation in column 2 showed rapid increases in amplitude with slow and monotonic decay, while those in column 4 displayed no rapid increase (Fig. 5*Ab*,*Ac*). The time-to-peak and the half-duration of the optical responses in L3 in the stimulated column 2 were 13 ± 1 and 91 ± 21 ms, respectively ($n = 5$; Fig. 5*Ab*,*Ac*). In the presence of capsaicin, however, the initial responses in columns 1–3 were followed by a second and third wave, whereas such waves observed in column 4 were not preceded by any initial sharp com-

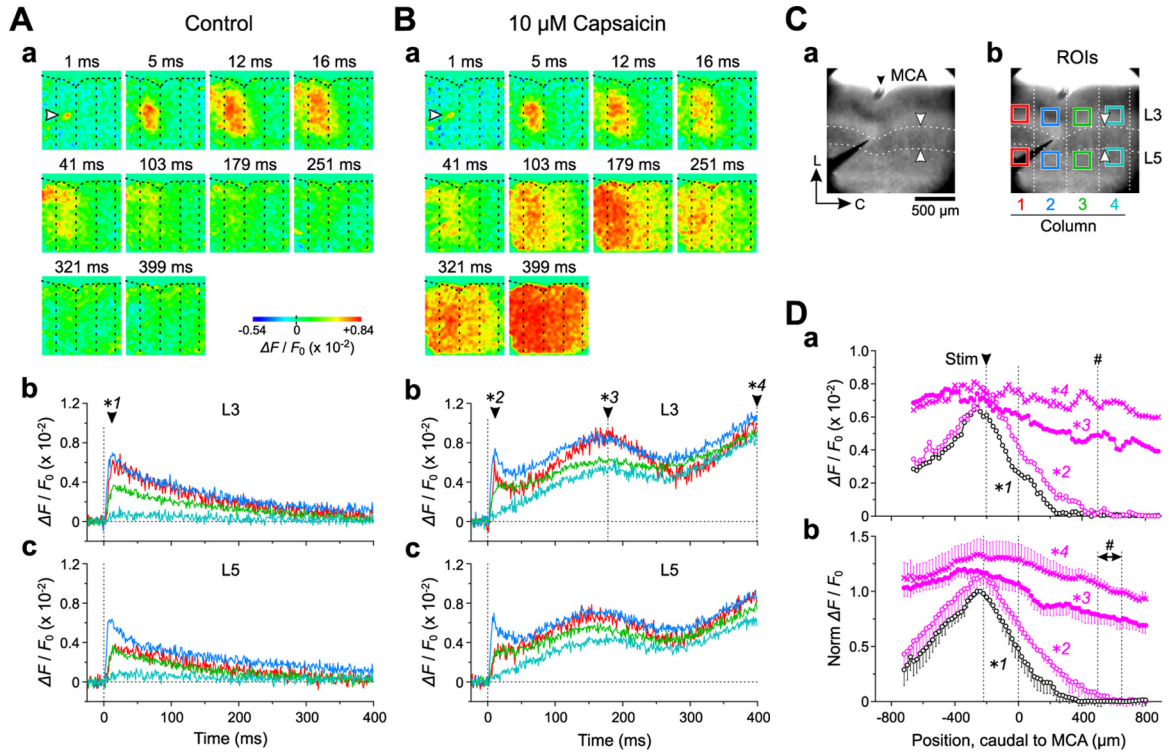

Figure 5. Oscillatory synchronization between Gu-I and Au-I induced by L4 stimulation in the presence of capsaicin. ***Aa***, ***Ba***, Sample pseudocolor images of optical responses induced by 4 μA (=1.2 × Th*) L4 stimulation in the absence (***Aa***) and presence (***Ba***) of 10 μM capsaicin. The arrowheads indicate the initial optical responses evoked in L4 with a latency of 1 ms. The vertical dotted lines showing the presumed column boundaries: The four columns were assigned numbers 1–4 from left to right (***Cb***). ***Ab***, ***Ac***, ***Bb***, ***Bc***, Temporal profiles at ROIs in L3 (***b***) and L5 (***c***) in columns 1–4 represented by red, blue, green, and cyan traces, respectively, in the absence (***A***) and presence (***B***) of capsaicin. The filled arrowheads indicate the peak time points of the initial responses (*1 and *2) and the second wave (*3) and the end point of the recording time window (*4). ***C***, Bright-field images of Gu-I. Stimulating electrode placed at 200 μm rostral to MCA (filled arrowhead) in L4 in Gu-I (***a***). A pair of facing open arrowheads indicates the boundary between Gu-I (DI) and Au-I (GI/DI). The vertical dotted lines indicate presumed column boundaries (***b***). The colored squares placed in L3 and L5 in columns 1–4 represent ROIs (***b***). The traces representing temporal profiles in columns 1–4 (***Ab***, ***Ac***, ***Bb***, ***Bc***) are colored in accordance with the colors of ROIs in columns 1–4. L, Lateral; C, caudal. ***Da***, Horizontal spatial profiles of the optical response in L3 at the time point of *1 (black circles) shown in ***Ab*** and at the time points of *2 (purple open circles), *3 (purple filled circles), and *4 (purple crosses) shown in ***Bb***. The pound sign (#) indicates the position of the border between Gu-I and Au-I. ***Db***, Averaged (±SD) horizontal spatial profiles ($n = 5$) in L3 at the peak time points of the initial sharp responses in the absence and presence of capsaicin (black and purple open circles, respectively), and at the peak time point of the second wave and the end point of the recording time window in the presence of capsaicin (purple filled circles and crosses, respectively). The pound sign (#) indicates the positions of the borders between Gu-I and Au-I ranging from 500 to 650 μm caudal to MCA.

ponent (Fig. 5*Bb*,*Bc*). The time-to-peak of the initial response and the peak time of the second wave of the temporal profiles in L3 in the stimulated column 2 were 11 ± 1 and 160 ± 12 ms, respectively ($n = 5$).

As seen in the horizontal spatial profiles of the optical responses in L3 (Fig. 5*Da*,*Db*) at the peak time points of the initial responses in the stimulated column in the absence (12 ms; Fig. 5*Ab*, *1) and presence (11 ms; Fig. 5*Bb*, *2) of capsaicin, the amplitudes of the initial optical responses declined to almost zero as the measuring point was moved toward the region of Au-I (black and purple open circles). However, at the peak time point of the second wave (179 ms, *3) and at the end of the recording time window (399 ms, *4) (Fig. 5*Bb*), the amplitudes of the optical responses at the caudal end of column 4 remained considerable (Fig. 5*Da*,*Db*, purple filled circles and crosses). Thus, the excitation initiated in column 2 of Gu-I by L4 stimulation propagated into more rostral and caudal columns with repetition of the excitation surges, leading to an oscillation-like synchronization across the entire Gu-I (columns 1–3) and at least the rostral portion of Au-I (column 4).

Capsaicin-induced oscillation leads to synchronization between Gu-I and Au-I

We next examined whether stronger stimulation (6 μA = 1.8 × Th*) could induce a direct excitation spread from Gu-I to Au-I in the absence of capsaicin. In response to 6 μA stimulation, a larger optical response was induced (5–11 ms) both in the absence and presence of capsaicin (Fig. 6*Aa*,*Ba*) in 7 of the 12 slices examined (58%) compared with the columnar pattern evoked by 1.2 × Th* stimulation (Fig. 5*Aa*,*Ba*, 5–12 ms). The larger initial optical response rapidly faded out in the absence of capsaicin (Fig. 6*Aa*, 27 ms), whereas in the presence of capsaicin, it was followed by a second and third excitation spread extending toward the caudal end of the imaged area of the insular cortex (Fig. 6*Ba*, 140–400 ms) in five of the seven slices. Given that the columnar width would not markedly vary among slices, we expediently divided the imaged area into four columns (Fig. 6*Aa*,*Ba*, vertical dotted lines). As revealed in the temporal profiles (Fig. 6*Ab*,*Bb*), sharply increasing responses were observed in columns 1–3 of Gu-I, whereas a much smaller delayed response was observed in column 4. The initial response obtained with 1.8 × Th* stimulation decayed much more rapidly compared with those obtained with 1.2 × Th* stimulation (Fig. 5*Ab*), as revealed by a significant ($^{\dagger}p < 0.001$) difference in half-duration (1.8 × Th* vs 1.2 × Th*; 24 ± 11 ms, $n = 5$, vs 91 ± 21 ms, $n = 5$). This finding suggests that the excitation induced by the stronger stimulation might have been immediately followed by inhibition; thus, the direct excitation spread from Gu-I to Au-I would be suppressed despite the application of stronger stimulation.

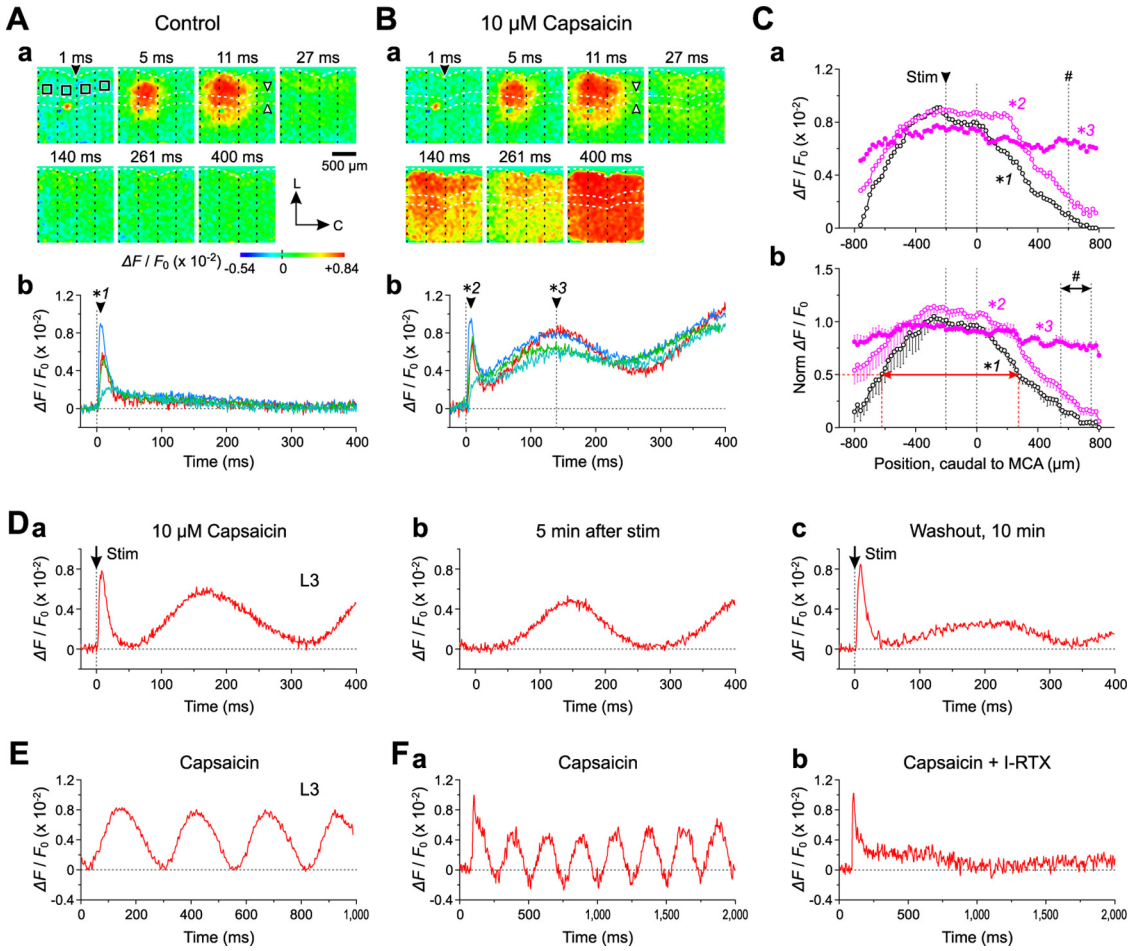

Figure 6. Facilitation of oscillatory synchronization between Gu-I and Au-I by stronger L4 stimulation. ***Aa***, ***Ba***, Sample pseudocolor images of optical responses induced in the absence (***A***) and presence (***B***) of 10 μM capsaicin by 6 μA (=1.8 × Th*) L4 stimulation applied to a site 200 μm rostral to MCA (filled arrowheads) in L4 of Gu-I in a slice with the boundary (open arrowheads) between Gu-I (DI region) and Au-I (GI/DI region) at 600 μm caudal to MCA. The vertical dotted lines showing the presumed column boundaries. The four columns were assigned numbers 1–4 from left to right. The black squares represent ROIs in columns 1–4. L, Lateral; C, caudal. ***Ab***, ***Bb***, Temporal profiles at L3 ROIs in columns 1–4 represented by red, blue, green, and cyan traces, respectively, in the absence (***Ab***) and presence (***Bb***) of capsaicin. The filled arrowheads indicate the peak time points of the initial responses (*1 and *2) and the second wave (*3). ***Ca***, Horizontal spatial profile of the optical response in L3 at the time point of *1 (black circles) shown in ***Ab*** and at the time points of *2 (purple open circles) and *3 (purple filled circles) shown in ***Bb***. The pound sign (#) indicates the position of the border between Gu-I and Au-I. ***Cb***, Averaged (±SD) horizontal profiles ($n = 5$) at the peak time points of the initial sharp response in the absence and presence of capsaicin (black and purple open circles, respectively) and at the peak time points of the second waves in the presence of capsaicin (purple filled circles). The pound sign (#) indicates the positions of the borders between Gu-I and Au-I ranging from 550 to 750 μm caudal to MCA. Red left–right arrow indicates the half-width of the horizontal profile. ***D***, A representative example of an initial sharp response followed by a slow oscillation induced in the presence of 10 μM capsaicin by 6 μA L4 stimulation (***a***). Persistence of the oscillation 5 min after single stimulation (***b***). Marked diminution of the slow oscillation following the unaltered initial response 10 min after capsaicin washout (***c***). ***E***, Once triggered, the oscillation persisted as long as capsaicin (5 μM) was present. ***F***, I-RTX (0.5 μM) addition to the perfusate including capsaicin (10 μM) abolished the capsaicin-induced oscillatory response, leaving the initial response unaffected (***a***, ***b***).

Indeed, as revealed in the horizontal spatial profiles in L3 (Fig. 6*Ca*,*Cb*, *1, black circles) at the peak time point of the initial sharp response (*1; 10 ± 1 ms; $n = 5$; Fig. 6*Ab*), the amplitude that peaked at the center of column 2 declined to almost zero toward the caudal end of column 4, despite the significantly larger ($^{\dagger}p < 0.005$) half-width (860 ± 42 μm; $n = 5$) of the horizontal spatial profile compared with that (588 ± 49 μm; $n = 5$) obtained with the weaker stimulation (Fig. 5*Db*). Similarly, in the presence of capsaicin, the amplitude at the peak time point of the initial sharp response (Fig. 6*Bb*, *2) declined markedly toward the caudal end of column 4 (Fig. 6*Ca*, *2). However, after the oscillation-like response was induced by the application of capsaicin, the amplitude of the optical responses at the peak time point of the second wave did not decline markedly even at the caudal end of column 4 (Fig. 6*Ca*, *3). The divergence in the amplitude of the second wave of oscillation-like responses among the four ROIs was considerably smaller compared with that induced with 1.2 × Th* stimulation (compare Figs. 5*Bb*, 6*Bb*). This result was consistent with a significant ($^{\dagger}p < 0.02$) difference in the percentile decline of amplitude at 800 μm caudal to MCA between the horizontal profiles of the second waves obtained with 1.2 × Th* (38 ± 6%; $n = 5$; Fig. 5*Db*) and 1.8 × Th* intensities (25 ± 3%; $n = 5$; Fig. 6*Cb*). This finding suggests that a stronger stimulation could facilitate the capsaicin-induced excitation spread from Gu-I to Au-I.

Once the oscillation-like response was induced by the presence of capsaicin following L4 stimulation (Fig. 6*Da*), it persisted for at least 15 min in most cases ($n = 8$ of 10; Fig. 6*Db*,*E*) and was markedly attenuated 10 min after washout of capsaicin (Fig. 6*Dc*). The time interval between the two given points that were located separately in the two rising phases of the optical responses and have an identical amplitude was almost constant in Figure 6, *Da* and *Db*, and was the same between Figure 6, *Da* and *Db*. This notion suggests the presence of the periodicity of the optical re-

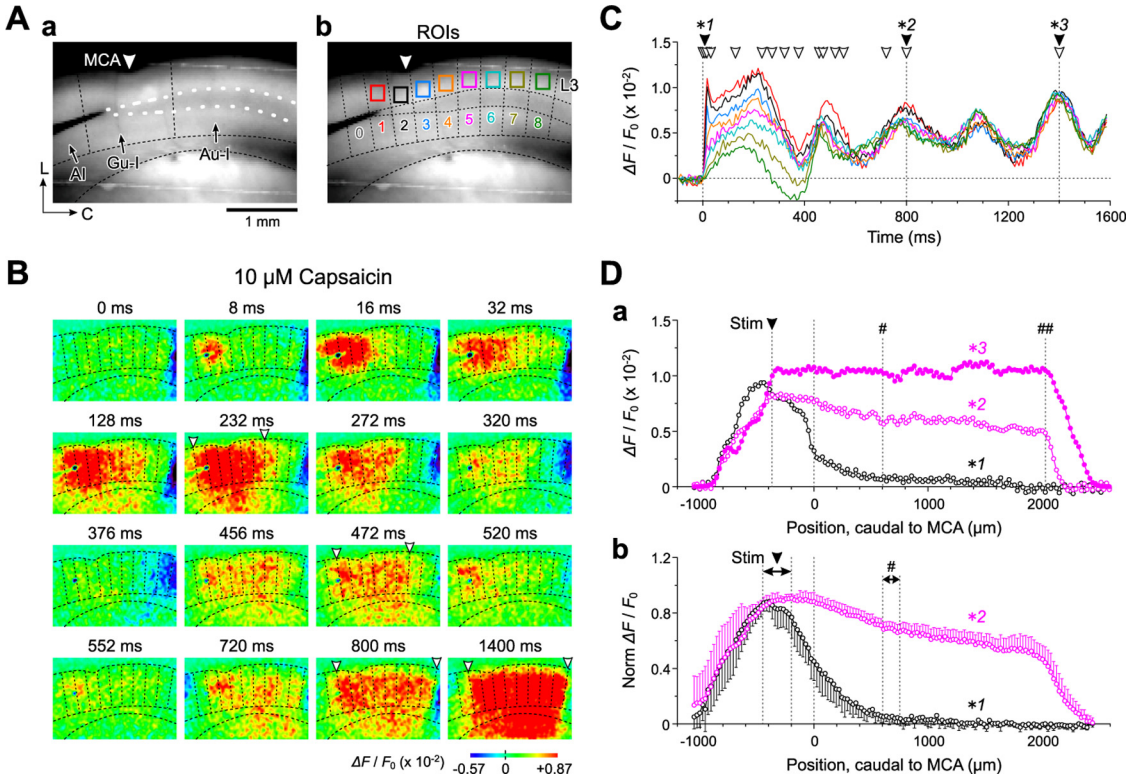

Figure 7. Synchronous oscillation between Gu-I and Au-I in the presence of capsaicin. ***A***, Resting-light-intensity images of the insular cortex in the tilted-horizontal slice. Stimulating electrode placed at L4 (400 μm rostral to MCA) of Gu-I (***a***). AI, agranular insula. The vertical dotted lines showing the presumed column boundaries (***b***). The colored squares representing ROIs in L3 of Gu-I (columns 1–3), Au-I (columns 5–8), and the Gu-I/Au-I boundary area (column 4). L, Lateral; C, caudal. ***B***, Sample pseudocolor images of optical responses evoked by stimulation of Gu-I L4 at 6 μA (=1.8 × Th*) in the presence of 10 μM capsaicin. The arrowheads indicate the rostral and caudal ends of columnwise excitation spread. ***C***, Traces representing temporal profiles at respective ROIs in columns 1–8 in the presence of capsaicin are colored in accordance with respective colors of ROIs in columns 1–8. The open arrowheads indicate the time points at which the respective pseudocolor-images (***B***) were obtained. The filled arrowheads indicate the peak time points of the initial responses (*1) and the fourth (*2) and sixth (*3) waves. ***Da***, Horizontal spatial profiles of the optical response in L3 at the time points of *1 (black circles), *2 (purple open circles), and *3 (purple filled circles) shown in ***C***. The pound sign (#) indicates the position of the border between Gu-I and Au-I. The double pound sign (##) indicates the position of the caudal end of Au-I. ***Db***, Averaged (±SD) horizontal profiles ($n = 5$) at 8 ms and the peak time point of the fourth wave (black and purple circles, respectively). The arrowhead and the pound sign (#) indicate the range of the positions of the stimulation sites and that of the positions of the borders between Gu-I and Au-I ranging from 600 to 750 μm caudal to MCA, respectively.

sponses. The mean periodicity was at 3.8 ± 0.1 Hz ($n = 8$). In the five slices examined, an addition of I-RTX (0.5 μM) to the perfusate containing capsaicin (10 μM) consistently abolished the capsaicin-induced oscillatory response, leaving the initial response unaffected (Fig. 6*Fa*,*Fb*). Thus, the oscillatory synchronization between Gu-I and Au-I was induced through the activation of TRPV1.

Capsaicin induces oscillatory network synchronization between Gu-I and Au-I

We further examined how far the oscillatory excitation initiated in Gu-I propagates beyond the boundary between Gu-I and Au-I using a system that captures optical responses in Gu-I (DI region) and the entire Au-I (GI/DI region) (Fig. 1*Ca*, the rectangular area labeled MC) at a sampling rate of 125 Hz. Due to this limited sampling rate, the peak amplitude of the initial sharp response would be underestimated in these experiments.

Stimulation of L4 in Gu-I at 6 μA (=1.8 × Th*; Fig. 7*Aa*) in the presence of 10 μM capsaicin induced an initial optical response with a columnar spatial pattern in Gu-I at 8 ms (Fig. 7*B*). Thereafter, the oscillatory optical response extended over Gu-I and Au-I (Fig. 7*B*). A similar oscillatory excitation spread was observed in a total of five of the eight slices examined. By referring to the apparent boundaries of the respective optical responses in Gu-I (Fig. 7*B*), we divided the imaged area into nine columns (columns 0–8; Fig. 7*Ab*). Because the boundary between DI and GI/DI was located at ~600 μm caudal to MCA within column 4 (Fig. 7*Aa*), Gu-I was represented in columns 1–3 and Au-I was represented in columns 5–8 (Fig. 7*Ab*). The optical response initiated in Gu-I column 1 rapidly spread caudally to column 3 (8–16 ms) and slowly propagated to columns 4–6 (232 ms) (Fig. 7*B*). This rapid spread within Gu-I was reflected in the rapid rise to the initial peak of the temporal profiles at the ROIs in columns 1–3, and the slow propagation into Au-I was reflected in the slow rising phases of those in columns 4–8 (Fig. 7*C*). This slow rise of the optical responses in Au-I (columns 4–6) peaked at 200–230 ms, almost simultaneously with the second wave of the optical responses in Gu-I (columns 1–3) (Fig. 7*C*).

Following the decay of those optical responses, the synchronized oscillatory response emerged after 400 ms following stimulation (Fig. 7*B*,*C*). During the first cycle of the oscillation (<400 ms), the amplitude of the optical responses was highest in the stimulated column 1 (Fig. 7*C*, red trace) and was smaller at more distant ROIs (Fig. 7*B*,*C*). However, as the oscillation progressed, the amplitude divergence in the optical responses among the columns gradually decreased (Fig. 7*C*), and the caudal end of the excited region shifted to the caudal end of Au-I (bregma −0.5 mm ≈ 2.0 mm caudal to MCA). Thus, a more widespread synchronous oscillation was induced over Gu-I and Au-I (Fig. 7*B*, 800 ms), which was more clearly observed in the wide-range

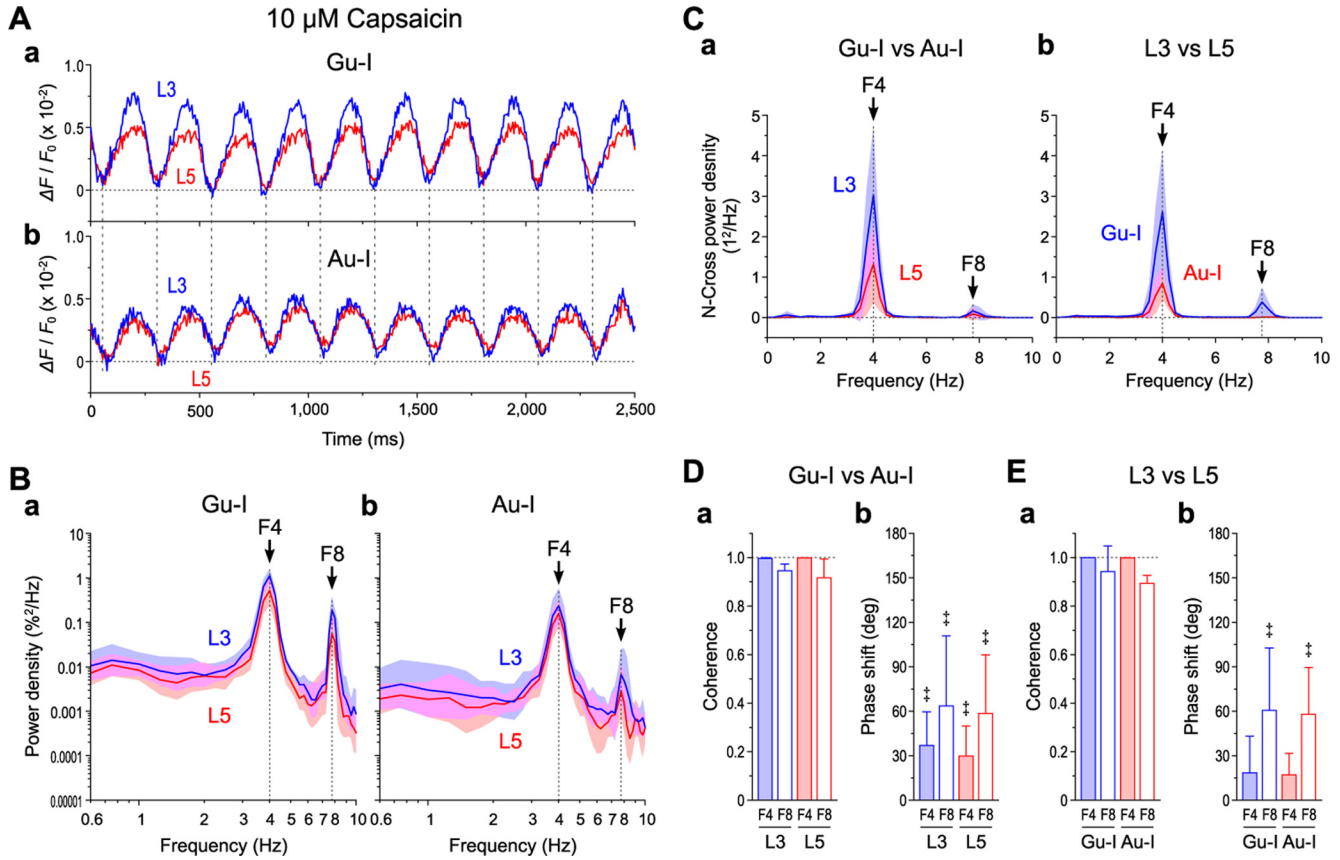

Figure 8. Theta synchronization between Gu-I and Au-I. ***A***, Examples of temporal profiles of long-lasting oscillatory optical responses triggered by 6 μA (=1.8 × Th*) Gu-I L4 stimulation in the presence of 5 μM capsaicin. Temporal profiles at ROIs located in L3 (blue traces) and L5 (red traces) of Gu-I (***a***) and those of Au-I (***b***) were simultaneously obtained. The vertical dotted lines indicate the timing of negative peaks of Gu-I L3 responses (250 ms interval). ***B***, Geometric mean (× [geometric SD]$^{\pm 1}$) power densities of the oscillatory responses in L3 (blue curves) and L5 (red curves) of Gu-I (***a***) and those of Au-I (***b***) ($n = 5$). ***C***, Mean (±SD) cross-power densities between Gu-I and Au-I in L3 (blue curve) and L5 (red curve) (***a***) and those between L3 and L5 in Gu-I (blue curve) and Au-I (red curve) (***b***) ($n = 5$). ***D***, ***E***, Mean (±SD) values of coherence (***a***) and phase shift (***b***) between F4 and F8 components of Gu-I and those of Au-I (***D***) and between those of L3 and those of L5 (***E***) ($n = 5$). $^{\ddagger}p < 0.05$ (vs 0°). Coherence between Gu-I and Au-I: L3 F4, 0.998 ± 0.003; L3 F8, 0.946 ± 0.026; L5 F4, 0.998 ± 0.001; L5 F8, 0.916 ± 0.078. Coherence between L3 and L5: Gu-I F4, 0.999 ± 0.001; Gu-I F8, 0.941 ± 0.107; Au-I F4, 0.998 ± 0.002; Au-I F8, 0.894 ± 0.032. Phase shift between Gu-I and Au-I: L3 F4, 37 ± 23°; L3 F8, 64 ± 47°; L5 F4, 30 ± 20°; L5 F8, 59 ± 39°. Phase shift between L3 and L5: Gu-I F4, 19 ± 25°; Gu-I F8, 61 ± 42°; Au-I F4, 17 ± 14°; Au-I F8, 58 ± 32°.

plateau-like horizontal profile of the optical response (Fig. 7*Da*, *2) at the peak time point of the fourth wave (Fig. 7*C*, *2). The fourth wave was the earliest cycle required for the optical response to reach the caudal end of Au-I (Fig. 7*Da*, ##), as shown in the averaged horizontal spatial profile (Fig. 7*Db*) obtained at the peak time point of the fourth wave (peak time, 812 ± 55 ms; $n = 5$). Together with the results shown in Figures 5 and 6, it is likely that TRPV1-assisted excitation in Gu-I initiates the oscillatory coordination of neural activity between Gu-I and Au-I, suggesting the presence of functional integration between Gu-I and Au-I.

Theta-band synchronization between Gu-I and Au-I

The wave of capsaicin-induced oscillatory optical responses that persisted for a long time (≥15 min) after Gu-I L4 stimulation (Fig. 8*A*) (see also Figs. 6*E*,*F*, 7*C*) appeared not to be a simple sine wave. In each cycle of the waves in Gu-I and Au-I, the onset of a positive wave in Gu-I preceded that in Au-I (vertical interrupted lines), indicating an excitation spread from Gu-I to Au-I. The power spectral analysis of temporal profiles of the oscillatory optical responses in Gu-I and Au-I ($n = 5$) revealed that the oscillation was mainly composed of two prominent frequency components of 3.5–4.5 Hz (F4) and 7–9 Hz (F8) (Fig. 8*Ba*,*Bb*). Both F4 and F8 powers were significantly larger ($^{\ddagger}p < 0.05$) in L3 than in L5 in Gu-I but not in Au-I ($^{\ddagger}p > 0.3$), while both F4 and F8 powers were also larger ($^{\ddagger}p < 0.02$) in Gu-I than in Au-I.

As oscillatory synchronization between Gu-I and Au-I was apparent (Figs. 5–7), we performed a cross-power spectral analysis to evaluate the degree of synchronization between Gu-I and Au-I. The cross-power densities (Sklar et al., 1972) between Gu-I and Au-I in both L3 ($^{\ddagger}p < 0.03$) and L5 ($^{\ddagger}p < 0.05$) were prominent at 4 Hz ($n = 5$; Fig. 8*Ca*), as were the cross-power densities between L3 and L5 in both Gu-I ($^{\ddagger}p < 0.03$) and Au-I ($^{\ddagger}p < 0.02$) ($n = 5$; Fig. 8*Cb*). Consistent with these observations, the coherence (Sklar et al., 1972) between Gu-I and Au-I in both L3 and L5 was very high (≈ 1) at 4 Hz but slightly lower (≈0.9) at 8 Hz ($n = 5$; Fig. 8*Da*), as was the coherence between L3 and L5 in both Gu-I and Au-I ($n = 5$; Fig. 8*Ea*). There were significant positive phase shifts between F4 in Gu-I and that in Au-I in both L3 and L5 ($^{\ddagger}p < 0.05$), between F8 in Gu-I and that in Au-I in both L3 and L5 ($^{\ddagger}p < 0.05$) (Fig. 8*Db*), and between F8 in L3 and that in L5 in both Gu-I and Au-I ($^{\ddagger}p < 0.05$) (Fig. 8*Eb*). A smaller and insignificant ($^{\ddagger}p > 0.08$) shift was observed between F4 in L3 and that in L5 in both Gu-I and Au-I (Fig. 8*Eb*). Thus, TRPV1 activation induced oscillatory synchronization between Gu-I and Au-I at the theta range as reflected in F4 and F8 components, and each

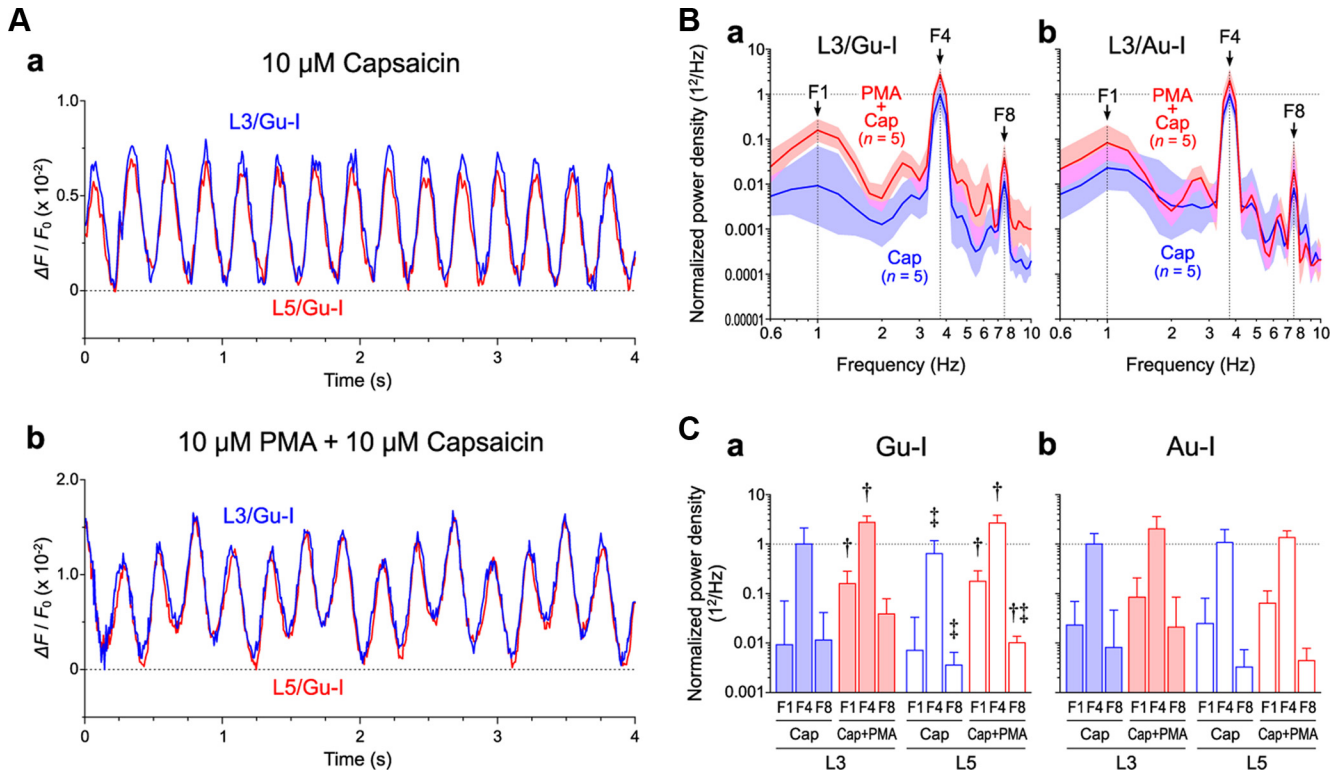

Figure 9. PMA-induced complex oscillations composed of 1, 4, and 8 Hz waves. ***A***, A simple (***a***) and a complex (***b***) oscillation induced by 4 μA (=1.2 × Th*) Gu-I L4 stimulation in L3 (blue traces) and L5 (red traces) of the stimulated column in Gu-I of two different slice preparations after bath application of 10 μM capsaicin alone and after bath application of 10 μM capsaicin in the presence of 10 μM PMA, respectively. ***B***, Geometric mean (× [geometric SD] $^{\pm 1}$) power densities of the oscillatory responses in the presence of capsaicin without (blue curves) and with PMA (red curves) in L3 of Gu-I ($n = 5$ and 5, respectively) (***a***) and Au-I ($n = 5$ and 5, respectively) (***b***). Optical responses in Gu-I and Au-I were obtained separately and nonpairwise. ***C***, Geometric mean (× [geometric SD] $^{\pm 1}$) values of F1, F4, and F8 power densities in L3 and L5 of Gu-I (***a***) and Au-I (***b***). The blue and red columns represent geometric mean power densities in the presence of capsaicin alone and with PMA, respectively. PMA significantly enhanced F1 and F4 components in L3 (solid columns) as well as in L5 (hollow columns) in Gu-I. $^{\dagger}p < 0.05$ (vs Cap); $^{\ddagger}p < 0.05$ (vs L5). Normalized values of the geometric mean (× [geometric SD] $^{\pm 1}$) F1, F4, and F8 in Gu-I; L3/Cap ($n = 5$): 0.0093 × 7.6 $^{\pm 1}$, 1 × 2.1 $^{\pm 1}$, and 0.012 × 3.6 $^{\pm 1}$; L3/Cap+PMA ($n = 5$): 0.16 × 1.8 $^{\pm 1}$, 2.7 × 1.3 $^{\pm 1}$, and 0.038 × 2.0 $^{\pm 1}$; L5/Cap ($n = 5$): 0.0072 × 4.6 $^{\pm 1}$, 0.63 × 1.9 $^{\pm 1}$, and 0.0036 × 1.8 $^{\pm 1}$; L5/Cap+PMA ($n = 5$): 0.18 × 4.6 $^{\pm 1}$, 2.6 × 1.4 $^{\pm 1}$, and 0.010 × 1.3 $^{\pm 1}$. Normalized values of the geometric mean (× [geometric SD] $^{\pm 1}$) F1, F4, and F8 in Au-I; L3/Cap ($n = 5$): 0.023 × 3.0 $^{\pm 1}$, 1 × 1.6 $^{\pm 1}$, and 0.0081 × 5.8 $^{\pm 1}$; L3/Cap+PMA ($n = 5$): 0.084 × 2.5 $^{\pm 1}$, 2.0 × 1.8 $^{\pm 1}$, and 0.021 × 4.0 $^{\pm 1}$; L5/Cap ($n = 5$): 0.025 × 3.2 $^{\pm 1}$, 1.1 × 1.8 $^{\pm 1}$, and 0.0033 × 2.2 $^{\pm 1}$; L5/Cap+PMA ($n = 5$): 0.064 × 1.8 $^{\pm 1}$, 1.4 × 1.4 $^{\pm 1}$, and 0.0044 × 1.8 $^{\pm 1}$.

cycle of such oscillatory responses might be initiated in the supragranular layer of Gu-I.

PMA induced a complex oscillation composed of 1, 4, and 8 Hz waves

Because the PKC activation similarly enhanced the two distinct I_{cap} in L3 and L5 PCs (Fig. 4), we examined whether PMA modulates capsaicin-induced oscillations in Gu-I and Au-I. Optical responses in Gu-I and Au-I were obtained separately and nonpairwise. In the presence of 10 μM capsaicin alone, Gu-I L4 stimulation consistently triggered apparently simple oscillations at ~4 Hz in Gu-I (0.2–0.4 mm rostral to MCA) (Fig. 9*Aa*; $n = 5$), similar to the results shown in Figure 8. However, bath application of 10 μM capsaicin in the presence of 10 μM PMA induced complex oscillations (Fig. 9*Ab*). The power spectrum analysis (Fig. 9*Ba*,*Bb*, red curves) revealed that this complex oscillation was composed of the three frequency components of 3.5–4 Hz (F4), 7–8 Hz (F8), and 0.7–1.5 Hz (F1) in Gu-I ($n = 5$) and Au-I (1.5–2.0 mm caudal to MCA) ($n = 5$). To examine the effects of PMA on oscillation, all the power spectra obtained in the presence of capsaicin together with or without PMA were normalized to the geometric mean of the peak F4 obtained in the presence of capsaicin alone. In Gu-I, the geometric mean values of F1 and F4 power densities in L3 and L5 obtained in the presence of PMA and capsaicin ($n = 5$) were significantly larger ($^{\dagger}p < 0.05$) than those obtained in the presence of capsaicin alone ($n = 5$), while PMA significantly affected the F8 power densities in L5 ($^{\dagger}p < 0.02$) but not in L3 ($^{\dagger}p > 0.2$) (Fig. 9*Ba*,*Ca*). In contrast, none of the geometric mean values of F1, F4, and F8 power densities in Au-I were significantly affected by PMA ($^{\dagger}p > 0.05$; $n = 5$; Fig. 9*Bb*,*Cb*). Such differential effects of PMA between oscillations in Gu-I and Au-I were consistent with the differential distribution of TRPV1 between Gu-I and Au-I (Fig. 2*C*). Collectively, these results showed that the oscillatory synchronization between Gu-I and Au-I mainly at the theta range was induced by capsaicin regardless of the presence or absence of PMA.

Capsaicin does not modulate spike trains induced by current pulse injections

To understand the cellular mechanisms underlying the synchronized oscillations observed, we examined the effects of capsaicin on spike firings evoked in PCs of Gu-I. First, we characterized the firing properties of L3 and L5 PCs of Gu-I and examined the effects of 5 μM capsaicin on spike trains induced by current pulse injections. In the absence of capsaicin, spike trains induced in L3 PCs by injection of current pulses displayed spike frequency adaptation (Fig. 10*Aa*), whereas those induced in L5 PCs displayed little spike frequency adaptation (Fig. 10*Ba*), as revealed by the changes in interspike intervals (ISIs) during spike trains (Fig. 10*Ab*,*Bb*). Spike frequency adaptation could also be assessed by

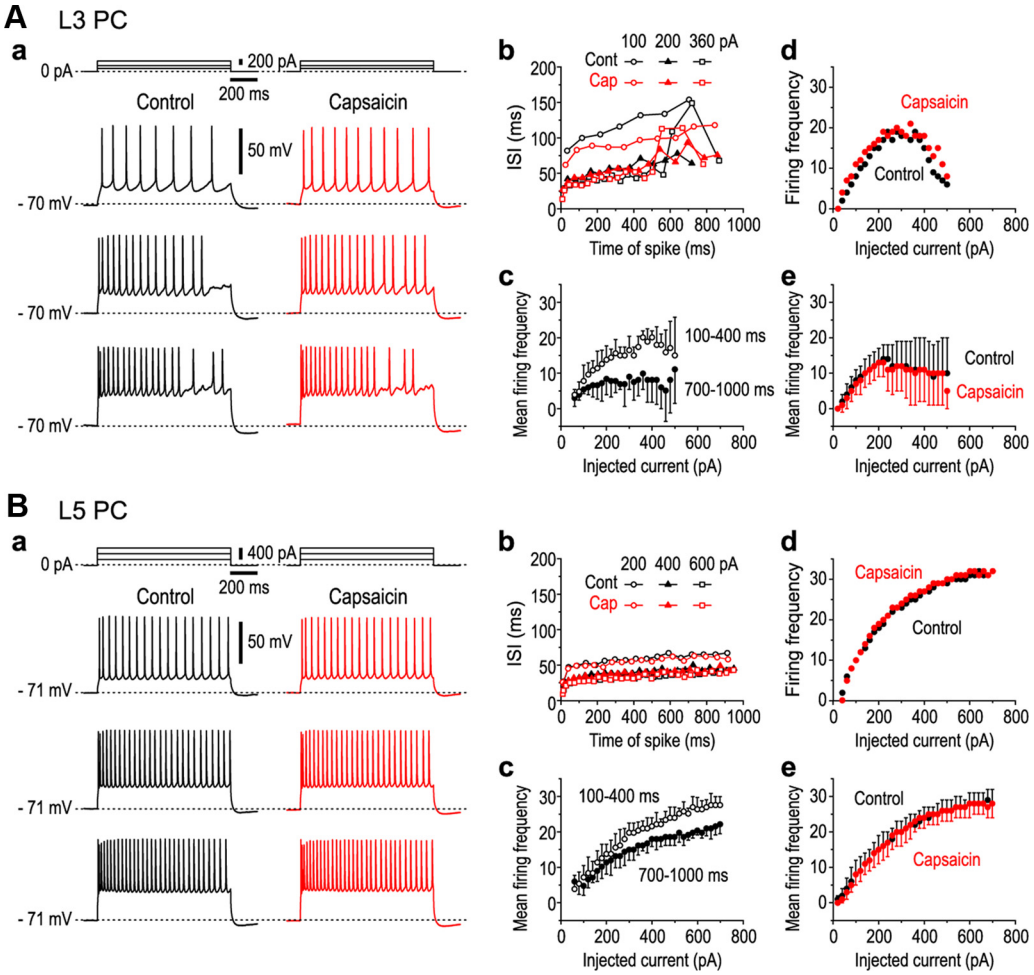

Figure 10. Effects of capsaicin on spike trains induced by current pulse injections. ***Aa***, ***Ba***, Sample traces of spike trains induced in an L3 PC (***Aa***) and in an L5 PC (***Ba***) by injection of current pulses with intensities of 100, 200, and 360 pA and with intensities of 200, 400, and 600 pA (top), respectively, in the absence (black traces) and presence (red traces) of 5 μM capsaicin. ***Ab***, ***Bb***, Plots of ISIs of the spike trains in the L3 and L5 PCs (shown in ***Aa*** and ***Ba***, respectively) against the time after the onset of current pulse with respective intensities. ***Ac***, ***Bc***, Relationships between the mean (±SD) firing frequencies and intensities of current pulses obtained during the time periods of 100–400 ms (open circles) and 700–1000 ms (filled circles) after the onset of the current pulse in the L3 ($n = 5$; ***Ac***) and L5 PCs ($n = 5$; ***Bc***). ***Ad***, ***Bd***, Relationships between firing frequencies and intensities of current pulses obtained during the entire duration of current pulses in the L3 and L5 PCs (shown in ***Aa*** and ***Ba***, respectively) in the absence (black circles) and presence (red circles) of capsaicin. ***Ae***, ***Be***, Relationship between the mean (±SD) firing frequencies and intensities of current pulses obtained during the entire duration of current pulses in L3 ($n = 5$; ***Ae***) and L5 PCs ($n = 5$; ***Be***) in the absence (black circles) and presence (red circles) of capsaicin.

the difference between the mean spike frequency during the time section of 100–400 ms and that during 700–1000 ms (Fig. 10*Ac*,*Bc*). The L3 PCs displayed prominent differences at any current intensities (Fig. 10*Ac*), whereas the L5 PCs displayed little differences up to 220–230 pA and thereafter showed differences (Fig. 10*Bc*). The differences observed at the current intensities ranging between 300 and 500 pA were significantly larger ($^{\$}p < 0.04$) in L3 PCs ($n = 6$) than that in L5 PCs ($n = 5$). With an increase in the intensity of injected currents, the mean firing frequency in L3 PCs increased but soon reached a maximum plateau (18 ± 4 Hz) at 200–500 pA (Fig. 10*Ae*) and occasionally decreased thereafter (Fig. 10*Ad*); however, that in L5 PCs increased to 28 ± 3 Hz at 600 pA (Fig. 10*Bd*,*Be*). These observations suggest that the excitability of L5 PCs is ~1.6 times higher than that of L3 PCs. Following application of 5 μM capsaicin, the resting membrane potential was significantly depolarized from −70 ± 3 to −67 ± 3 mV in the L3 PCs ($^{\ddagger}p < 0.001$; $n = 6$) but remained almost unchanged in the L5 PCs (−69 ± 1 vs −69 ± 2 mV; $^{\ddagger}p > 0.2$; $n = 5$). The two distinct firing patterns caused in L3 and L5 PCs by current pulse injections remained virtually unchanged with the application of capsaicin. There was no significant (L3, $^{\$}p > 0.8$; L5, $^{\$}p > 0.9$) difference in the mean firing frequency before and after the application of capsaicin in L3 and L5 PCs (Fig. 10*Ae*,*Be*). However, this result does not preclude the possibility that capsaicin modulates spike firing evoked by synaptic activation.

Capsaicin modulates spike firings evoked by synaptic activation

In response to L4 stimulation (2–3 μA) that causes only local optical responses instead of a columnar spatial pattern in Gu-I, an L3 PC displayed a transient burst of spikes riding over the slow depolarization envelope (Fig. 11*Aa*, top, *). In the presence of 5 μM capsaicin, the same stimulation induced a similar transient burst of spikes (*) and subsequent spike firings that appeared to be triggered from vigorous bombardments of EPSPs (Fig. 11*Ab*, top), as shown in the enlarged trace (Fig. 11*Ab*, bottom). Such vigorous bombardments of EPSPs were consistently observed only in the presence of capsaicin in the five L3 PCs examined. The mean number of spikes and the mean spike frequency measured during the capsaicin-induced additional spike firings were 9 ± 4 and 4.4 ± 2.4 Hz, respectively ($n = 5$) (Fig. 11*Ac*, gray area). In

contrast, in the five L5 PCs examined, capsaicin neither induced EPSP bombardment nor depolarized the resting membrane potential, but enhanced the transient burst firing evoked by L4 stimulation (Fig. 11, compare *Ba*, *Bb*). The mean number of spikes measured during the transient burst firing was significantly ($^{\ddagger}p < 0.05$, $n = 5$) increased from 9 ± 2 to 15 ± 3, while the mean spike frequency was insignificantly ($^{\ddagger}p > 0.1$, $n = 5$) increased from 13 ± 4 to 18 ± 3 Hz (Fig. 11*Bc*). Such an enhancement was pronounced at the first stimulation but progressively declined in response to subsequent stimulations, presumably due to the tachyphylaxis of TRPV1 responses. Thus, transient bursts induced by a weak L4 stimulation (2–3 μA) were either prolonged in L3 or enhanced in L5 PCs by capsaicin, but only to <2–3 s.

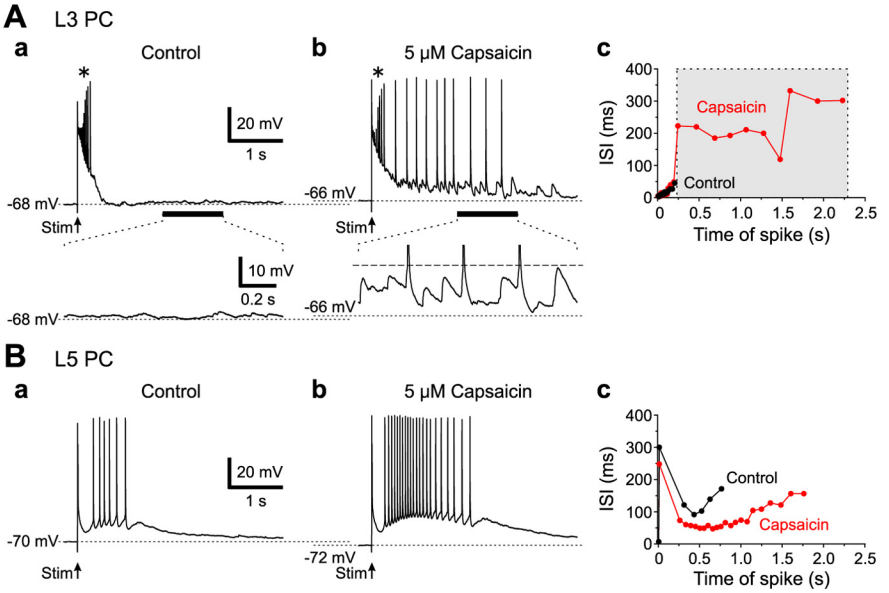

Figure 11. Effects of capsaicin on spike firings evoked by stimulation of L4 in L3 and L5 PCs of Gu-I. ***A***, Top, Spike firings induced in an L3 PC evoked by 2.5 μA L4 stimulation in the absence (***a***) and presence (***b***) of 5 μM capsaicin. The asterisk (*) denotes a transient burst commonly observed in ***a*** and ***b***. Bottom, Enlarged traces of the responses (horizontal bars, top), showing the absence (***a***) and presence (***b***) of vigorous EPSP. The interrupted line indicates the spike threshold (***b***). Plots of ISIs of the spike trains in the L3 PC in the absence (black circles) and presence (red circles) of capsaicin against the time after the onset of stimulation (***c***). Spike firings induced by capsaicin (gray area). ***B***, Spike firings induced in an L5 PC evoked by 2.5 μA L4 stimulation in the absence (***a***) and presence (***b***) of capsaicin. Plots of ISIs of the spike trains in the L5 PC in the absence (black circles) and presence (red circles) of capsaicin against the time after stimulation (***c***). Shown is the enhancement of transient burst firings by capsaicin.

Capsaicin induces enormously sustained rhythmic firings at 4 Hz in L3 PCs

We next addressed what firing patterns govern L3 and L5 PCs during the oscillatory optical response triggered by stimulation of L4 in Gu-I at 4–6 μA in the presence of capsaicin (Figs. 5–7). In response to stimulation of L4 in Gu-I at 4–6 μA in the presence of capsaicin, sustained firings with varying durations were induced in a total of 75 L3 PCs located within the stimulated column (Fig. 12*Ba*). The cumulative frequency histogram of durations of sustained firings observed in all the L3 PCs displayed a steep increase followed by a much slower increase (Fig. 12*Aa*, black continuous curve). A curve fitting (red dotted curve) of the cumulative frequency histogram with an integration of the sum of two normal distribution functions revealed the presence of short and long duration groups, which were represented as the two distinct cumulative probability distributions (K-S test, $p < 0.001$; Fig. 12*Aa*, black dotted and interrupted curves, respectively). The L3 PCs of the long duration group thus determined ($n = 24$) displayed enormously sustained spike firings (≥108 s; Fig. 12*Ab*, gray columns), which persisted for 311 ± 124 s (Fig. 12*Ba*,*D*). High-amplitude oscillatory fluctuations of membrane potential (Fig. 12*Ba*, *) were usually observed after the cessation of the sustained spike firing, suggesting the occurrence of vigorous bombardments of EPSPs, similar to the results shown in Figure 11*Ab*. In 10 of the 24 L3 PCs constituting the long-duration group, sustained spike firings were rhythmic as shown on an expanded timescale (Fig. 12*Bb*), and persisted for 351 ± 170 s. The autocorrelogram of the entire spike train (Fig. 12*Ba*) revealed that the spike activity occurred with a periodicity of 0.26 ± 0.04 s ($n = 10$; Fig. 12*Bc*). This periodicity was more clearly observed in the early phase of sustained spike firings (Fig. 12*Ba*, blue bar; *Bd*).

However, clear periodicity was not observed in most of the 51 L3 PCs constituting the short-duration group (28 ± 18 s; Fig. 12*Ab*, hollow columns; *D*). This observation suggests that the duration of sustained firings would be more prolonged as periodicity becomes more apparent. Thus, the rhythmic firing may be sustained depending on the strength of synaptic connectivity between the recorded L3 PC and surrounding PCs that display network oscillatory activities. Not only the duration of sustained firings in the long group but also that in the short group L3 PCs was significantly longer ($^{\dagger}p < 0.001$) than that observed in the absence of capsaicin (9 ± 4 s; $n = 11$; Fig. 12*Ca*,*D*), and also significant longer ($^{\dagger}p < 0.001$) than that observed after coapplication of capsaicin with 0.5 μM I-RTX (11 ± 6 s; $n = 14$; Fig. 12*Cb*,*D*). Thus, the sustained rhythmic firing at 4.0 ± 0.6 Hz ($n = 10$) observed in L3 PCs is likely to be induced through the activation of TRPV1, consistent with the F4 component observed in the oscillatory optical responses (Fig. 8*Ba*, blue curve).

Capsaicin induces short-lived sustained rhythmic firings at 8 Hz in L5 PCs

Stimulation of L4 in the presence of capsaicin induced sustained firings with varying durations in a total of 21 L5 PCs located within the stimulated column. Similar to the case with L3 PCs (Fig. 12*A*), a curve fitting of the cumulative frequency histogram of durations of sustained firings revealed the presence of two subgroups; the short-lived (49 ± 20 s; $n = 9$) and transient (11 ± 3 s; $n = 12$) groups (Fig. 13*A*,*F*). In six of the nine L5 PCs constituting the short-lived group, sustained firings were rhythmic with a mean periodicity of 0.13 ± 0.01 s (Fig. 13*Ba–Bc*), which was significantly shorter ($^{\dagger}p < 0.001$) than that observed in L3 PCs (Fig. 12*Bc*,*Bd*). However, periodicity was not clearly observed in the 12 L5 PCs constituting the transient group. The sustained firing persisted only for 7 ± 3 s ($n = 5$) in the absence of capsaicin (Fig. 13*C*), which was significantly shorter ($^{\dagger}p < 0.001$ and $^{\dagger}p < 0.03$) than those in the short-lived and transient groups (Fig. 13*F*). Thus, the short-lived sustained and rhythmic firings at 8.0 ± 0.7 Hz ($n = 6$) observed in the L5 PCs is likely to be induced through the activation of TRPV1, consistent with the F8 component (Fig. 8*Ba*). The duration of sustained firings in the short-lived group in the L5 PCs was approximately six times shorter

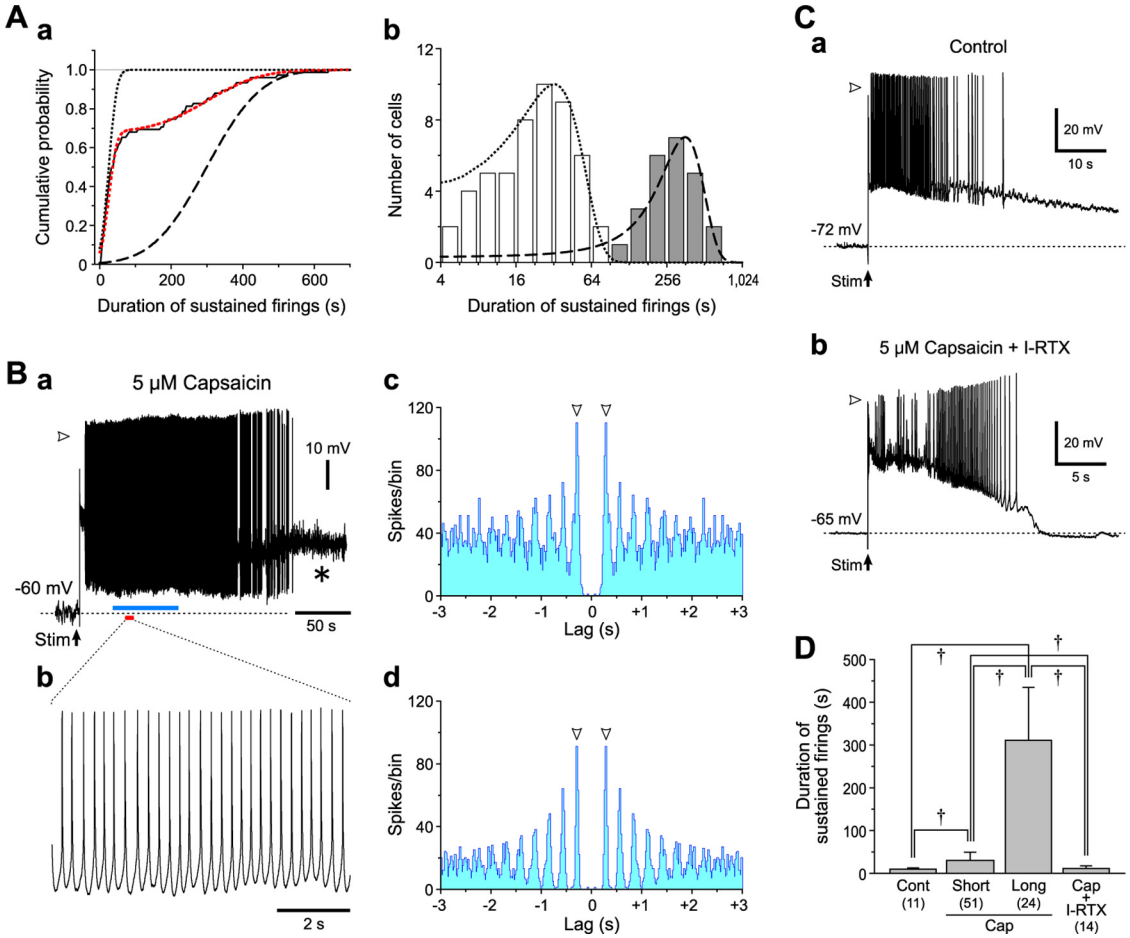

Figure 12. Sustained spike firings in L3 PCs. ***A***, A cumulative frequency histogram of durations of capsaicin-induced sustained firings observed in 75 L3 PCs (***a***). The black continuous and red dotted curves represent a cumulative frequency histogram and its approximation by a cumulative distribution function of the sum of two normal distributions, respectively. The black dotted and interrupted curves represent the cumulative probability distributions in the short and long duration groups, respectively, between which there was a significant difference (K-S test, $p < 0.001$). A histogram of firing durations with a logarithmic bin width; $(\sqrt{2})^{i+4} - (\sqrt{2})^{i+3}$ s for *i*th bin (***b***). The hollow and gray columns represent the short- and long-duration groups, respectively. The two normal distributions were illustrated with the same curves as those applied in ***a***. ***B***, Sustained spike firings induced in an L3 PC evoked by 6 μA L4 stimulation in the presence of 5 μM capsaicin (***a***). The asterisk (*) denotes high-amplitude membrane potential fluctuations. The arrowhead indicates a membrane potential level of 0 mV (***a***). Expanded traces of spike firings (red bar, ***a***) (***b***). Autocorrelograms of the spike train in the entire period of sustained spike firing (***c***) and in its early episode (blue bar, ***a***) (***d***) showing the same periodicity of 0.29 s (arrowheads). Bin width, 20 ms. ***C***, Spike firings induced in L3 PCs by stimulation of L4 with an intensity of 6 μA in the absence of capsaicin (***a***) and in the presence of capsaicin and 0.5 μM I-RTX (***b***). The arrowheads indicate a membrane potential level of 0 mV. ***D***, Mean (+SD) burst durations obtained in L3 PCs under the respective conditions. $^{\dagger}p < 0.001$. Cont, 9 ± 4 s ($n = 11$); Cap Short, 28 ± 18 s ($n = 51$); Cap Long, 311 ± 124 s ($n = 24$); Cap+I-RTX, 12 ± 6 s ($n = 14$).

($^{\dagger}p < 0.001$) than that in the long group observed in the L3 PCs (Fig. 12*D*).

Because PMA removed the desensitization of TRPV1 in L5 PCs and enhanced TRPV1 responses in L3 PCs that project to L5 PCs (Fig. 4), PMA would prolong the duration of sustained rhythmic firing in L5 PCs. Indeed, the rhythmic firing induced in the presence of PMA and capsaicin by L4 stimulation persisted for a much longer time (293 ± 109 s) in 7 of the 19 L5 PCs examined (Fig. 13*Da*,*F*). Unexpectedly, four of the seven L5 PCs examined displayed rhythmic firings with long periodicities (0.25 ± 0.02 s; Fig. 13*Db*,*Dc*), instead of the shorter one seen in the presence of capsaicin alone. In the remaining three L5 PCs, the ISI during the sustained firing increased gradually (Fig. 13*Ea*), and the periodicity also increased from 0.12 ± 0.02 s in the initial period (<200 s) to ~0.25 ± 0.02 s in the late period (>200 s) (Fig. 13*Eb*,*Ec*).

PMA also induced a longer periodicity of 1.35 ± 0.09 s ($n = 5$) (Fig. 13*Dc*,*Eb*, filled arrowhead), which appeared to interfere with shorter periodicities. As the time lag increased toward the peak of the longer periodicity, the peak density of the shorter periodicity was reduced (Fig. 13*Dc*,*Eb*), presumably due to the disturbance of the short periodicity through interspersed slow firing. These results indicate that L5 PCs display a periodicity of 8.0 ± 0.7 Hz in the presence of capsaicin alone, whereas they display altered or additional periodicity of 4.1 ± 0.3 Hz together with a further slower one of 0.7 ± 0.05 Hz in the presence of PMA and capsaicin.

Discussion

There is rapidly accumulating evidence that TRPV1 is widely expressed in various brain regions, suggesting its crucial role in brain function (Kauer and Gibson, 2009), but highly restricted distribution of TRPV1 in the CNS has recently been reported as well using *Trpv1* reporter mice (Cavanaugh et al., 2011). This discrepancy could be due to the underestimation of reporter molecules attached to TRPV1, which is expressed at a much lower level in the CNS than in the DRG. Although the insular cortices display a higher level of TRPV1 among brain regions, the role of TRPV1 remained unknown. We demonstrated the critical roles

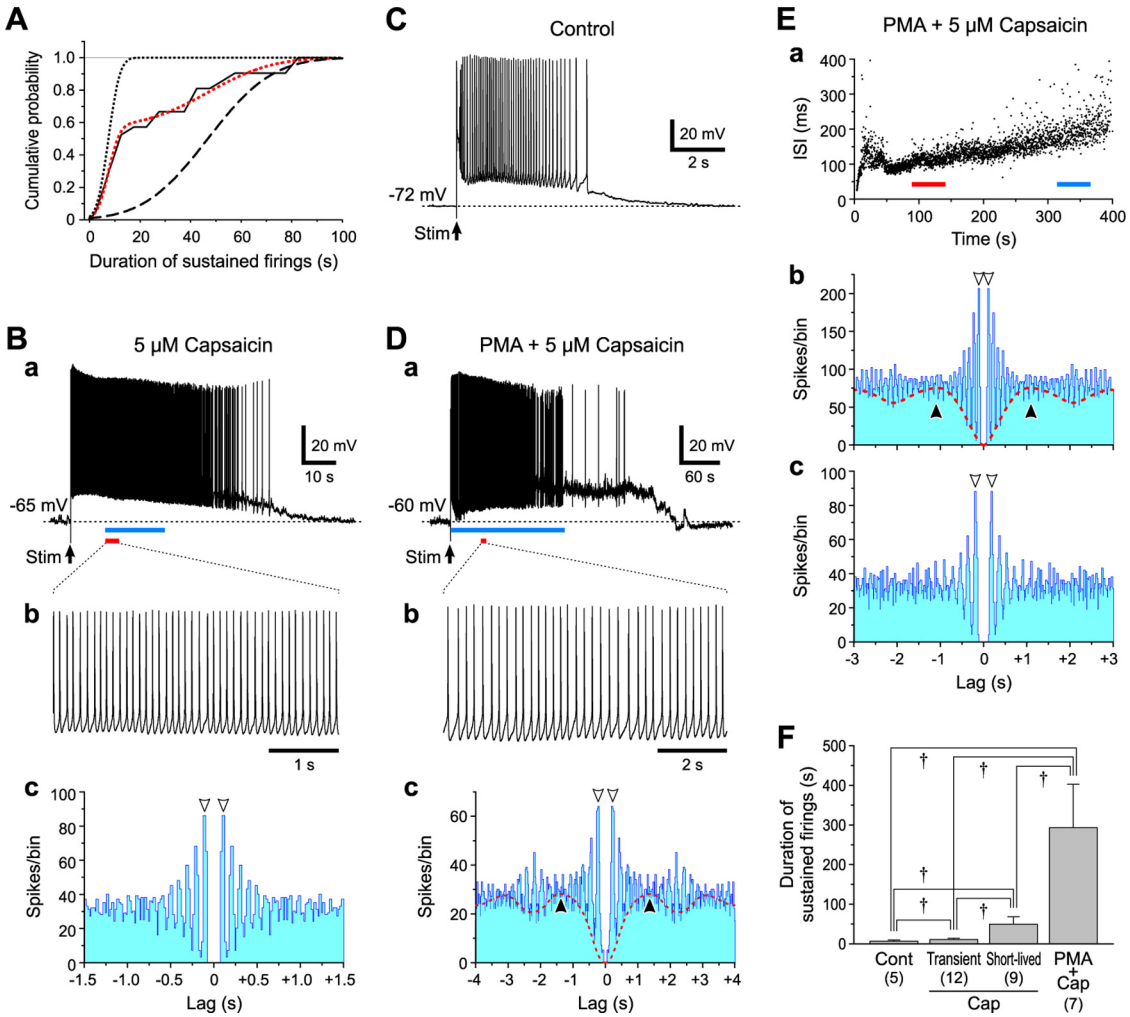

Figure 13. Sustained spike firings in L5 PCs. ***A***, A cumulative frequency histogram of durations of capsaicin-induced sustained firings observed in 21 L5 PCs. The black continuous and red dotted curves represent a cumulative frequency histogram and its approximation by a cumulative distribution function of the sum of two normal distributions, respectively. The black dotted and interrupted curves represent the cumulative probability distributions in the short- and long-duration groups, respectively, between which there was a significant difference (K-S test, $p < 0.001$). ***B***, Sustained spike firings induced in an L5 PC evoked by 6 μA L4 stimulation in the presence of 5 μM capsaicin (***a***). Expanded traces of spike firings (red bar, ***a***) (***b***). Autocorrelogram of the spike train (blue bar, ***a***) showing a periodicity of 0.11 s (arrowheads) (***c***). Bin width, 20 ms. ***C***, Spike firings induced in an L5 PC evoked by 6 μA L4 stimulation in the absence of capsaicin. ***D***, Sustained spike firings induced in an L5 PC evoked by 6 μA L4 stimulation in the presence of PMA and capsaicin (***a***). An expanded trace of spike firings (red bar, ***a***) (***b***). Autocorrelogram of the spike train (blue bar, ***a***) showing two periodicities of 0.23 (open arrowheads) and 1.3 s (filled arrowheads) (***c***). Bin width, 20 ms. ***E***, Plot of ISIs during sustained spike firing against the time after stimulation in an L5 PC evoked in the presence of PMA and capsaicin (***a***). Autocorrelograms of the spike trains (red and blue bars, ***a***) showing shorter (0.13 s, ***b***) and longer (0.25 s, ***c***) periodicities (open arrowheads). The autocorrelogram (***b***) also revealed a further longer periodicity of ~1 s (filled arrowheads) in the L5 PC. Bin width, 20 ms. ***F***, Mean (+SD) burst durations obtained in L5 PCs under respective conditions. $^{\dagger}p < 0.03$. Cont, 7 ± 3 s ($n = 5$); Cap Transient, 11 ± 3 s ($n = 12$); Cap Short-lived, 49 ± 20 s ($n = 9$); PMA+Cap, 293 ± 109 s ($n = 7$).

of TRPV1 in inducing theta-band synchronization between the gustatory and autonomic insular cortices.

Possible columnar integration in Gu-I and its modulation by capsaicin

It has been reported that, during taste administrations in rats, Gu-I displays network oscillations at 7–12 Hz persisting for ~2 s (Tort et al., 2010) and distinct spatial patterns of neural ensemble activities over a large cortical region (~3 mm^2) depending on taste quality (Yamamoto, 1987; Accolla et al., 2007). In the present study, in the horizontal slice preparations of Gu-I, the stimulation of L4 at 1.2 × Th* caused stereotyped optical responses, which displayed monophasic temporal profiles with half-durations of 91 ± 21 ms (Fig. 5*Ab*) and columnar spatial profiles with half-widths of 588 ± 49 μm (Fig. 5*Db*; $n = 5$). These temporal and spatial profiles were similar ($^{\dagger}p > 0.1$ and $^{\dagger}p > 0.3$) to those (half-durations, 71 ± 20 ms; half-widths, 491 ± 83 μm; $n = 14$) obtained by stimulation at 1.2 × Th* in the coronal slice preparations of Gu-I [partly from the study by Sato et al. (2008)], in which the presence of the functional column as a unitary local circuit was firmly established as follows: Stimulation of L3 or L5 in the presence of picrotoxin as well as that of L4 in the absence of picrotoxin caused the excitation that invariably spreads vertically across layers uniformly [Sato et al. (2008), their Figs. 8, 9], thus inducing a stereotyped columnar spatial pattern, regardless of the stimulation site in Gu-I. Although the columnar spatial pattern may not necessarily reflect the classically defined functional column such as orientation or ocular dominance columns (Hubel and Wiesel, 1962), both types of columns serve as a functional unit. Such temporal and spatial profiles of excitation spreads, evoked by electrical stimulation, were much shorter and narrower than the temporal and spatial profiles of responses to taste stimulations (Yamamoto, 1987; Accolla et al., 2007), suggesting that taste stimulations cause distinct integrations among several

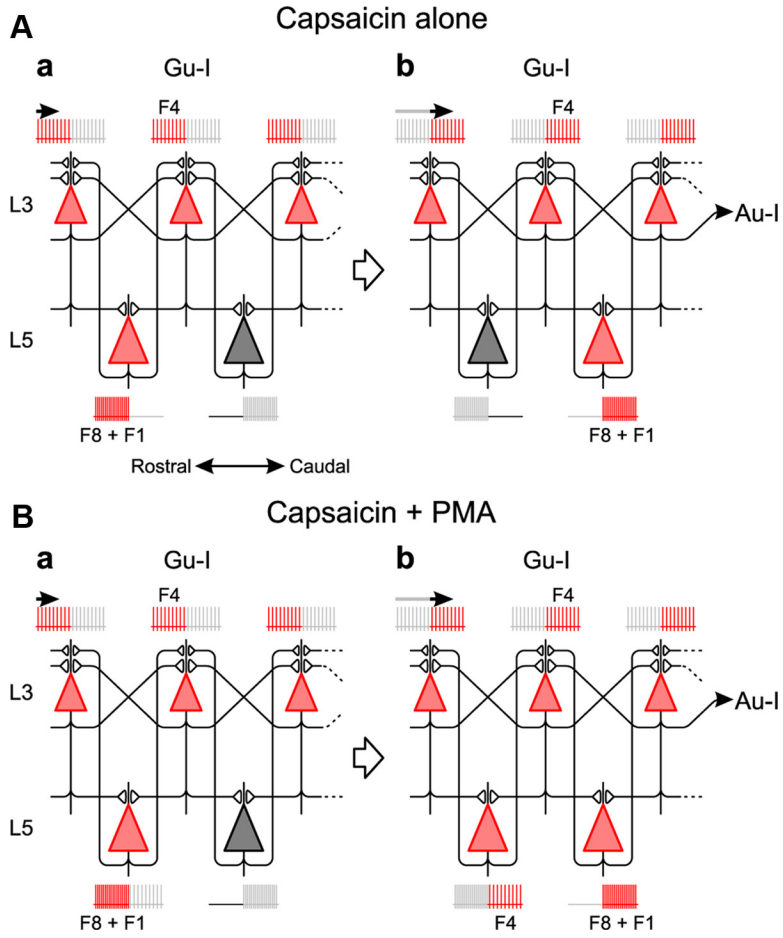

Figure 14. Possible network for theta-band synchronization. ***A***, Sustained rhythmic firing at 4 Hz in L3 PCs generated by recurrent network among L3 PCs in the presence of capsaicin. A short-lived rhythmic firing at 8 Hz occurs alternately in adjacent L5 PCs during the sustained rhythmic firing in L3 PCs. Such network oscillations propagate from Gu-I to Au-I. Red and gray represent the present and future (***a***) or the present and past (***b***) activities, respectively. ***B***, Enhancement of recurrent network synchronization among L3 PCs by coapplication of PMA and capsaicin engages L5 PCs in the same theta-band synchronization after a short-lived 8 Hz firing. Red and gray represent the present and future (***a***) or the present and past (***b***) activities, respectively.

columns in Gu-I depending on the taste quality. Surprisingly, capsaicin altered the monophasic optical response, confined in a single column, to the oscillatory response at theta-band rhythm, causing synchronization among multiple columns across Gu-I and Au-I (Figs. 5–7). These spatial profiles exceeded those induced by the four basic tastants (Accolla et al., 2007).

Functional coupling between Gu-I and Au-I by theta oscillation

Theta oscillations (4–12 Hz) occur in the hippocampus during memory-guided movement as well as during learning and memory (Hasselmo, 2005). These theta oscillations are often divided into two types (Kramis et al., 1975; Buzsáki, 2002): Type I occurs at slightly higher frequencies (6–12 Hz) and is associated with motor activity, whereas type II occurs at the lower frequencies (4–9 Hz) and is associated with the processing of sensory stimuli before initiating motor activity. In the present study, L5 PCs primarily displayed a short-lived 8 Hz oscillation (Fig. 13*B*,*F*), while L3 PCs mostly displayed a sustained 4 Hz oscillation (Fig. 12*B*) in response to stimulations of Gu-I L4 in the presence of capsaicin. In Gu-I and Au-I, as L5 and L3 PCs are involved in motor control and sensory processing, respectively (Yamamoto et al., 1988; Yasui et al., 1991; Hanamori et al., 1998), 8 Hz oscillation in L5 PCs and 4 Hz oscillation in L3 PCs are consistent with the natures of type I and type II theta oscillations, respectively, and are consistent with the differential firing characteristics of these neurons such that the excitability of L5 PCs was ~1.6 times higher than that of L3 PCs (Fig. 10).

TRPV1 was mostly detected in the postsynaptic dendritic spines that received asymmetrical synapses in the insular cortex. As there are much less dendritic spines in GABAergic inhibitory neurons (GABA-INs) compared with pyramidal cells, pyramidal cells would be primarily involved in the generation of capsaicin-induced theta oscillation. Furthermore, the capsaicin-induced oscillation was not abolished by picrotoxin (figure not shown). However, it is still possible that GABA-INs are involved in the synchronization of pyramidal cells activities, provided that GABA-INs have reciprocal synaptic connections with pyramidal cells that express $GABA_B$ receptors, as demonstrated in the thalamus (Kim et al., 1997).

The coapplication of capsaicin and PMA altered L5 PCs to display sustained rhythmic firings composed of 1 and 4 Hz components, instead of or after the short-lived 8 Hz oscillation (Fig. 13*D*,*E*). It is possible that an enhancement of the synchronization among L3 PCs by PMA engaged more L5 PCs in the same 4 Hz oscillation as that in L3 PCs through the interaction between L3 and L5 PCs because the synchronization mechanism among L3 PCs is much more potent than that among L5 PCs (Fig. 14) [Sato et al. (2008), their Fig. 9]. In agreement with this hypothesis, PMA significantly enhanced F4 and F1 components not only in L3 but also in L5 in Gu-I (Fig. 9*Ba*,*Ca*). These findings are consistent with the fact that both L3 and L5 PCs have their presynaptic terminals in both L3 and L5. Together, it is likely that, in L3 or L5, a large fraction of the F4 component and most of the F8 component of oscillatory optical responses reflect synaptic actions evoked in L3 or L5 by the activities of L3 and L5 PCs that fire rhythmically at 4 and 8 Hz, respectively. The F1 component and some remaining fraction of the F4 component are likely to be mediated by the activity of L5 PCs. Au-I stimulation never induced the oscillatory synchronization between Gu-I and Au-I, presumably because the TRPV1 density in L2/3 was five times lower in Au-I than in Gu-I (Fig. 2*C*).

Oscillations recorded from different brain regions become synchronized to form a large-scale network for the integration of distributed brain function (Varela et al., 2001; Fujisawa and Buzsáki, 2011). Therefore, the theta-band neural synchronization between Gu-I and Au-I that was demonstrated by cross-power spectral analysis (Fig. 8) might suggest the presence of functional integration between Gu-I and Au-I. Impulse activities arising from TRPV1-expressing terminals in taste buds and oral mucosa (Kido et al., 2003) and those in submucosa in the gastrointestinal tract (Ward et al., 2003) could ascend to layer 4 of Gu-I and Au-I, respectively, through the different thalamic nuclei (Cechetto and

Saper, 1987). This might result in oscillatory synchronization between Gu-I and Au-I, similar to those observed in the present study. Such synchronization might also be involved in the autonomic responses or, at least, modulate the responses caused by viscero-visceral reflexes. Although the endogenous ligands activating TRPV1 in PCs in the insular cortex are unknown, endocannabinoid may be a candidate for activating TRPV1 (Zygmunt et al., 1999).

Cellular mechanisms for capsaicin response

In Gu-I, TRPV1 was mostly expressed in the postsynaptic dendritic spines and was two times more densely expressed in L3 than in L5 (Fig. 2*C*). In L3 PCs, the activation of postsynaptic TRPV1 led to a vigorous bombardment of EPSPs (Fig. 11*Ab*), presumably reflecting a reinforcement of the synchronization mechanism among L3 PCs through their reciprocal connections. Subsequently, the prolonged sustained rhythmic firing was induced in L3 PCs by capsaicin (Fig. 12*B*). As TRPV1 in L3 PCs did not display Ca^{2+}-dependent desensitization (Fig. 3*A*) and was colocalized with asymmetrical synapses (Fig. 2*B*), TRPV1-mediated Ca^{2+} increases might have increased the surface expression of postsynaptic AMPA receptors, similar to the Ca^{2+}-dependent LTP of AMPA responses through NMDA receptor activation (Malenka and Bear, 2004). This idea is consistent with the report that TRPV1 colocalizes with PSD95 (Goswami et al., 2010), similar to the colocalization of NMDA with PSD95 (O'Brien et al., 1998).

In contrast, capsaicin enhanced the transient burst firing evoked in L5 PCs, but seldom induced EPSP bombardment (Fig. 11*Bb*), suggesting that transient Ca^{2+} influx through TRPV1 enhanced the possible Ca^{2+}-dependent burst (Haj-Dahmane and Andrade, 1997; Kang et al., 1998). Thus, capsaicin differentially modulated spike firings induced in L3 and L5 PCs by L4 stimulation, presumably due to the differential desensitization in capsaicin-induced current between L3 and L5 PCs (Fig. 3). The binding of Ca^{2+}-activated calmodulin to TRPV1 (Numazaki et al., 2003) and the activation of Ca^{2+}/calmodulin-dependent phosphatase (Jung et al., 2004) mediate the desensitization of TRPV1. In the rat insular cortex, calbindin-28 kDa was highly expressed in L3 compared with L5 (van Brederode et al., 1991; Paxinos et al., 2008). Therefore, the ability to chelate intracellular free Ca^{2+} may be much higher in L3 PCs than in L5 PCs, thereby suppressing the Ca^{2+}-dependent desensitization of TRPV1 responses in L3 PCs.

References

Accolla R, Bathellier B, Petersen CC, Carleton A (2007) Differential spatial representation of taste modalities in the rat gustatory cortex. J Neurosci 27:1396–1404. CrossRef Medline

Buzsáki G (2002) Theta oscillations in the hippocampus. Neuron 33:325–340. CrossRef Medline

Caterina MJ, Schumacher MA, Tominaga M, Rosen TA, Levine JD, Julius D (1997) The capsaicin receptor: a heat-activated ion channel in the pain pathway. Nature 389:816–824. CrossRef Medline

Cavanaugh DJ, Chesler AT, Jackson AC, Sigal YM, Yamanaka H, Grant R, O'Donnell D, Nicoll RA, Shah NM, Julius D, Basbaum AI (2011) Trpv1 reporter mice reveal highly restricted brain distribution and functional expression in arteriolar smooth muscle cells. J Neurosci 31:5067–5077. CrossRef Medline

Cechetto DF, Saper CB (1987) Evidence for a viscerotopic sensory representation in the cortex and thalamus in the rat. J Comp Neurol 262:27–45. CrossRef Medline

Cechetto DF, Saper CB (1990) Role of the cerebral cortex in autonomic functions. In: Central regulation of autonomic functions (Loewy AD, Spyer KM, eds), pp 208–223. New York: Oxford UP.

Dunér-Engström M, Fredholm BB, Larsson O, Lundberg JM, Saria A (1986) Autonomic mechanisms underlying capsaicin induced oral sensations and salivation in man. J Physiol 373:87–96. Medline

Fujisawa S, Buzsáki G (2011) A 4 Hz oscillation adaptively synchronizes prefrontal, VTA, and hippocampal activities. Neuron 72:153–165. CrossRef Medline

Ganong W (2003) Review of medical physiology, Ed 21. New York: McGraw-Hill Professional.

Goswami C, Rademacher N, Smalla KH, Kalscheuer V, Ropers HH, Gundelfinger ED, Hucho T (2010) TRPV1 acts as a synaptic protein and regulates vesicle recycling. J Cell Sci 123:2045–2057. CrossRef Medline

Grueter BA, Brasnjo G, Malenka RC (2010) Postsynaptic TRPV1 triggers cell type-specific long-term depression in the nucleus accumbens. Nat Neurosci 13:1519–1525. CrossRef Medline

Hachiya S, Kawabata F, Ohnuki K, Inoue N, Yoneda H, Yazawa S, Fushiki T (2007) Effects of CH-19 Sweet, a non-pungent cultivar of red pepper, on sympathetic nervous activity, body temperature, heart rate, and blood pressure in humans. Biosci Biotechnol Biochem 71:671–676. CrossRef Medline

Haj-Dahmane S, Andrade R (1997) Calcium-activated cation nonselective current contributes to the fast afterdepolarization in rat prefrontal cortex neurons. J Neurophysiol 78:1983–1989. Medline

Hanamori T, Kunitake T, Kato K, Kannan H (1998) Responses of neurons in the insular cortex to gustatory, visceral, and nociceptive stimuli in rats. J Neurophysiol 79:2535–2545. Medline

Hasselmo ME (2005) What is the function of hippocampal theta rhythm?—Linking behavioral data to phasic properties of field potential and unit recording data. Hippocampus 15:936–949. CrossRef Medline

Hubel DH, Wiesel TN (1962) Receptive fields, binocular interaction and functional architecture in the cat's visual cortex. J Physiol 160:106–154. Medline

Ishida Y, Ugawa S, Ueda T, Murakami S, Shimada S (2002) Vanilloid receptor subtype-1 (VR1) is specifically localized to taste papillae. Brain Res Mol Brain Res 107:17–22. CrossRef Medline

Jasmin L, Burkey AR, Granato A, Ohara PT (2004) Rostral agranular insular cortex and pain areas of the central nervous system: a tract-tracing study in the rat. J Comp Neurol 468:425–440. CrossRef Medline

Jung J, Shin JS, Lee SY, Hwang SW, Koo J, Cho H, Oh U (2004) Phosphorylation of vanilloid receptor 1 by Ca^{2+}/calmodulin-dependent kinase II regulates its vanilloid binding. J Biol Chem 279:7048–7054. CrossRef Medline

Kang Y, Okada T, Ohmori H (1998) A phenytoin-sensitive cationic current participates in generating the afterdepolarization and burst afterdischarge in rat neocortical pyramidal cells. Eur J Neurosci 10:1363–1375. CrossRef Medline

Kang Y, Dempo Y, Ohashi A, Saito M, Toyoda H, Sato H, Koshino H, Maeda Y, Hirai T (2007) Nitric oxide activates leak K^+ currents in the presumed cholinergic neuron of basal forebrain. J Neurophysiol 98:3397–3410. CrossRef Medline

Kauer JA, Gibson HE (2009) Hot flash: TRPV channels in the brain. Trends Neurosci 32:215–224. CrossRef Medline

Kido MA, Muroya H, Yamaza T, Terada Y, Tanaka T (2003) Vanilloid receptor expression in the rat tongue and palate. J Dent Res 82:393–397. CrossRef Medline

Kim S, Kang C, Shin CY, Hwang SW, Yang YD, Shim WS, Park MY, Kim E, Kim M, Kim BM, Cho H, Shin Y, Oh U (2006) TRPV1 recapitulates native capsaicin receptor in sensory neurons in association with Fas-associated factor 1. J Neurosci 26:2403–2412. CrossRef Medline

Kim U, Sanchez-Vives MV, McCormick DA (1997) Functional dynamics of GABAergic inhibition in the thalamus. Science 278:130–134. CrossRef Medline

Koplas PA, Rosenberg RL, Oxford GS (1997) The role of calcium in the desensitization of capsaicin responses in rat dorsal root ganglion neurons. J Neurosci 17:3525–3537. Medline

Kramis R, Vanderwolf CH, Bland BH (1975) Two types of hippocampal rhythmical slow activity in both the rabbit and the rat: relations to behavior and effects of atropine, diethyl ether, urethane, and pentobarbital. Exp Neurol 49:58–85. CrossRef Medline

Lee TS (1954) Physiological gustatory sweating in a warm climate. J Physiol 124:528–542. Medline

Malenka RC, Bear MF (2004) LTP and LTD: an embarrassment of riches. Neuron 44:5–21. CrossRef Medline

Mandadi S, Numazaki M, Tominaga M, Bhat MB, Armati PJ, Roufogalis BD

(2004) Activation of protein kinase C reverses capsaicin-induced calcium-dependent desensitization of TRPV1 ion channels. Cell Calcium 35:471–478. CrossRef Medline

Mandadi S, Tominaga T, Numazaki M, Murayama N, Saito N, Armati PJ, Roufogalis BD, Tominaga M (2006) Increased sensitivity of desensitized TRPV1 by PMA occurs through PKCε-mediated phosphorylation at S800. Pain 123:106–116. CrossRef Medline

Marinelli S, Di Marzo V, Berretta N, Matias I, Maccarrone M, Bernardi G, Mercuri NB (2003) Presynaptic facilitation of glutamatergic synapses to dopaminergic neurons of the rat substantia nigra by endogenous stimulation of vanilloid receptors. J Neurosci 23:3136–3144. Medline

Numazaki M, Tominaga T, Toyooka H, Tominaga M (2002) Direct phosphorylation of capsaicin receptor VR1 by protein kinase Cε and identification of two target serine residues. J Biol Chem 277:13375–13378. CrossRef Medline

Numazaki M, Tominaga T, Takeuchi K, Murayama N, Toyooka H, Tominaga M (2003) Structural determinant of TRPV1 desensitization interacts with calmodulin. Proc Natl Acad Sci U S A 100:8002–8006. CrossRef Medline

O'Brien RJ, Lau LF, Huganir RL (1998) Molecular mechanisms of glutamate receptor clustering at excitatory synapses. Curr Opin Neurobiol 8:364–369. CrossRef Medline

Paxinos G, Watson C (1998) The rat brain in stereotaxic coordinates, Ed 4. Amsterdam: Academic.

Paxinos G, Watson C, Carrive P, Kirkcaldie M, Ashwell K (2008) Chemoarchitectonic atlas of the rat brain, Ed 2. Amsterdam: Academic.

Roberts JC, Davis JB, Benham CD (2004) [^{3}H]Resiniferatoxin autoradiography in the CNS of wild-type and TRPV1 null mice defines TRPV1 (VR-1) protein distribution. Brain Res 995:176–183. CrossRef Medline

Rudenga K, Green B, Nachtigal D, Small DM (2010) Evidence for an integrated oral sensory module in the human anterior ventral insula. Chem Senses 35:693–703. CrossRef Medline

Ruggiero DA, Mraovitch S, Granata AR, Anwar M, Reis DJ (1987) A role of insular cortex in cardiovascular function. J Comp Neurol 257:189–207. CrossRef Medline

Sanchez JF, Krause JE, Cortright DN (2001) The distribution and regulation of vanilloid receptor VR1 and VR1 5′ splice variant RNA expression in rat. Neuroscience 107:373–381. CrossRef Medline

Sato H, Shimanuki Y, Saito M, Toyoda H, Nokubi T, Maeda Y, Yamamoto T, Kang Y (2008) Differential columnar processing in local circuits of barrel and insular cortices. J Neurosci 28:3076–3089. CrossRef Medline

Sklar B, Hanley J, Simmons WW (1972) An EEG experiment aimed toward identifying dyslexic children. Nature 240:414–416. CrossRef Medline

Tominaga M, Caterina MJ, Malmberg AB, Rosen TA, Gilbert H, Skinner K, Raumann BE, Basbaum AI, Julius D (1998) The cloned capsaicin receptor integrates multiple pain-producing stimuli. Neuron 21:531–543. CrossRef Medline

Tort AB, Fontanini A, Kramer MA, Jones-Lush LM, Kopell NJ, Katz DB (2010) Cortical networks produce three distinct 7–12 Hz rhythms during single sensory responses in the awake rat. J Neurosci 30:4315–4324. CrossRef Medline

Treede RD, Kenshalo DR, Gracely RH, Jones AK (1999) The cortical representation of pain. Pain 79:105–111. CrossRef Medline

van Brederode JF, Helliesen MK, Hendrickson AE (1991) Distribution of the calcium-binding proteins parvalbumin and calbindin-D28k in the sensorimotor cortex of the rat. Neuroscience 44:157–171. CrossRef Medline

Varela F, Lachaux JP, Rodriguez E, Martinerie J (2001) The brainweb: phase synchronization and large-scale integration. Nat Rev Neurosci 2:229–239. CrossRef Medline

Vellani V, Mapplebeck S, Moriondo A, Davis JB, McNaughton PA (2001) Protein kinase C activation potentiates gating of the vanilloid receptor VR1 by capsaicin, protons, heat and anandamide. J Physiol 534:813–825. CrossRef Medline

Ward SM, Bayguinov J, Won KJ, Grundy D, Berthoud HR (2003) Distribution of the vanilloid receptor (VR1) in the gastrointestinal tract. J Comp Neurol 465:121–135. CrossRef Medline

Yamamoto T (1987) Cortical organization in gustatory perception. Ann N Y Acad Sci 510:49–54. CrossRef Medline

Yamamoto T, Matsuo R, Kiyomitsu Y, Kitamura R (1988) Sensory inputs from the oral region to the cerebral cortex in behaving rats: an analysis of unit responses in cortical somatosensory and taste areas during ingestive behavior. J Neurophysiol 60:1303–1321. Medline

Yasui Y, Breder CD, Saper CB, Cechetto DF (1991) Autonomic responses and efferent pathways from the insular cortex in the rat. J Comp Neurol 303:355–374. CrossRef Medline

Zygmunt PM, Petersson J, Andersson DA, Chuang H, Sørgård M, Di Marzo V, Julius D, Högestätt ED (1999) Vanilloid receptors on sensory nerves mediate the vasodilator action of anandamide. Nature 400:452–457. CrossRef Medline